

Author Comment for revised manuscript acp-2020-55

Referee #3, Douglas Day

I commend the authors on their thorough explanations and modeling/text revisions in response to all of the reviewer comments. I believe the paper is greatly improved as a result of these efforts. It is interesting to see how much the oligomer contributions for α -pinene+NO₃ (Fig. 3) changed as a result of the model updates (i.e. adding in reversible vapor-wall loss, teflon diffusion, and increasing the accommodation coefficient).

Response: We thank Douglas Day very much for his critical and constructive reviews that enabled us to significantly improve the manuscript.

I recommend publication after one small detail is addressed.

In Section 2.2. where the revised manuscript now describes the description of the newly added vapor-wall interactions treatment (using the Huang et al. 2018 two-layer model), it states:

“The gas diffusion flux from the chamber interior to the wall near-surface gas phase $J_{dif,X,ws}$ is described using the Fickian gas diffusivity coefficient $D_{g,X}$ and an additional Eddy diffusivity coefficient k_e , which was estimated to be 0.03 s⁻¹ for the GTEC chamber in a previous study (Nah et al., 2016).”

However, I could not find in the Nah et al (2016) reference where the eddy diffusion rate constant of 0.03 s⁻¹ was estimated/reported (nor in the Nah et al., 2017 paper referenced elsewhere in the paper in case the year was simply listed incorrectly here). Maybe I just missed it and it is described in some context outside of vapor-wall loss. Can the authors please check that this citation is correct and includes this reported value? Or maybe it was just estimated according to the recommended equations in Krechmer et al. (2016) and Huang et al. (2018)?

Response: Please excuse this error due to a typo in the bibtex command. The eddy diffusion coefficient is reported in Nah et al. (2016a), not in (Nah et al., 2016b), see the corrected references below and in the revised manuscript.

Anonymous Referee #4

This manuscript presents a global optimization approach for assigning kinetic parameters to represent secondary organic aerosol (SOA) processes, including gas-phase chemistry, (equilibrium/non-equilibrium) gas/particle partitioning, and particle-phase chemistry. A number of additional processes that affect SOA formation and losses in chamber studies are represented, including diffusion and wall losses of gases and particles. The gas-phase chemical mechanism is based on the Leeds Master Chemical Mechanism, with addition of reactions/products to represent oxidation of the second double bond in limonene by NO₃. Parameters are obtained using the Monte Carlo Genetic Algorithm through a two-step inverse fitting procedure. Given the extreme complexity and nonlinearity of the processes that directly and indirectly affect observed SOA mass formation and yields in chambers (and ambient) studies, the problem of representing SOA formation is well suited to optimization methods and statistical modeling. This paper is novel and represents an important advancement in diagnostic modeling of SOA formation.

While many of the represented processes are known to occur, at least under some conditions, many are also poorly constrained. It is thus understood that given the large number of processes represented and parameters optimized in the model, a number of assumptions were needed. That said, the manuscript could be improved by evaluating the model results (parameter ranges and observed sensitivities) more broadly in the context of published literature. That the chamber experiments are generally well represented by the model, and in some cases only well represented with inclusion of specific processes, is important. However, that alone does not necessarily demonstrate the validity of the model approach; i.e., that the derived parameters are reasonable and are in general agreement with other observations when such comparisons can be made. At times the observed sensitivities are attributed to one process or parameter in the model, but a systematic discussion of whether the parameter range(s) are reasonable and those conclusions are more broadly supported in the literature is lacking. Some specific examples are provided below. This is acknowledged to some degree at the end of the paper (the verification of parameter values), but I think could be mitigated with better comparison to existing literature.

Response: We thank the anonymous referee very much for their time to produce this diligent review and their positive evaluation. We agree that the complexity of the system is high and there are challenges associated with balancing model accuracy, simplicity and flexibility. A general problem we face is that many parameters only make sense in the context of others. For example, a volatility distribution of product molecules will look different when oligomerization reactions are considered. To our knowledge, this is the first time both are determined in conjunction for the investigated systems. Hence, we cannot look at volatility distributions in the literature for comparison. In another example, branching ratios in the gas phase chemical mechanism between this study and the MCM template cannot be compared as easily because MCM does neither treat dimer formation from RO₂ + RO₂, nor oxidation of the second double bond of limonene. In general, organic nitrate formation is heavily underestimated in MCM-based calculations, so comparing to the published literature would not be constructive. We added discussions of these complications to the manuscript as detailed below.

We see this paper as a first-of-its-kind work that not only outlines possible avenues and provides scientific insights, but also leaves room to discuss the potential shortcomings of the modeling process. The manuscript already contained comparisons of the more uniquely defined parameters (e.g. oligomerization and oligomer decomposition rates, enthalpies of vaporization) and experimental observables (SOA yields, pON/OA) to literature values. However, upon initiative of the referee, we put even more emphasis on the discussion of

comparing derived parameters with literature constraints as outlined in the following point-by-point answers to the referee's comments.

While the manuscript is well written from a grammatical perspective, some of the technical writing needs improvement. Some specific examples are provided below. It is my general conclusion that this is an important paper that should be published in ACP, but some remaining technical issues need to be addressed.

Technical comments:

In line 280, the authors note that the number of parameter sets was likely not sufficient given the number of input parameters. What is rule for determining parameter sets, and what would be a more reasonable number?

Response: This is a tough question that likely has no simple answer as it depends on how well behaved the optimization hypersurface and how constrained the parameter space is. In these systems, the optimization hypersurface is non-convex, meaning that it occupies a large amount of local minima and there is no straight path to the global minimum. On the other hand, the optimization hypersurface will occupy multiple equivalent but non-identical global minima due to measurement data scatter and non-orthogonality of model parameters, making them statistically easier to find. From our experience, it would likely take a few million model runs, not just 150 000, to get consistent, reproducible results of optimizations with ~30 varied parameters, but we have not tested it for this specific case.

Using the method introduced by Donahue et al., VBS fits are only well constrained for bins within 1 order of magnitude of the observed SOA levels. For observed SOA mass levels of ~50-80 ug/m³, the assigned bins are outside this range. Is there something unique about the optimization and assignment method used that supports the bin ranges assigned and parameters obtained? The standard deviations shown in Fig. S4 suggest that the distributions vary widely between model runs (and thus are not well constrained). Further, if I understand Figs. 2b,c, the model suggests nearly all of the SOA mass is oligomeric and in the lowest volatility bin. This may explain the relative insensitivity to the initial volatility distribution (i.e., the similar measurement-model agreement achieved despite the significant differences in the volatility distributions obtained).

Response: The referee is correct that we lose some sensitivity to the initial volatility distribution when oligomerization chemistry is dominant. However, we also see that adding particle-phase chemistry extends the range of VBS bins that can be probed with a single chamber experiment towards higher volatilities. This is because an effective oligomerization reaction can lead to slow uptake of volatile monomer species that otherwise would partition only to an immeasurable extent into the particle phase. However, we also think volatility of these species and their oligomerization rate form a non-orthogonal parameter pair here: increasing oligomerization rate and shifting molecules to higher VBS bins may have a similar effect ("less molecules oligomerizing faster" vs "more molecules oligomerizing slower"). Hence, multiple solutions lead to very similar outcomes.

The discussion of Fig. 2c in the text (327) is confusing, as it states that Fig. 2c shows the “actual” volatility distribution in the particle phase. This suggests observational results, but the figure caption indicates model results. Further, the use of “actual” implies a disagreement between Fig. S4 and 2c., but they really represent different processes.

Response: The referee raises a very good point; usage of the word “actual” may suggest measurement results. We changed “actual volatility distribution of particle-phase organics” to

Line 329-330: *“resulting volatility distribution of organics in the particle phase according to the model”*

In other places, we have been vigilant with sentence fragments such as “the model suggests” or “in the model” to make it clear whether we talk about a result from inverse modelling or from experimental observation. We added another instance in line 429.

The discussion of the kinetic modeling results for alpha-pinene starting on line 104 is very hard to follow. I think the confusion stems from the statement that the gas-phase dimer “content” is increasing. The mass amount looks like it is staying the same, while the monomers are decreasing (evaporating), and thus the gas-phase dimers represent a greater fraction of the total condensed mass. That is more consistent with partitioning theory and Fig. 3b.

Response: The referee raises a good point. We rephrased the paragraph under avoidance of the term “gas-phase dimer content”.

“Upon increase in chamber temperature, the gas-phase dimer content increases considerably from 22 % to 74 % over the course of the experiment due to evaporation of monomers in volatility bins $C^ = 10\text{--}100 \mu\text{g}/\text{m}^3$ and decomposition of oligomers.”*

Now reads:

Lines 418-420: *“Upon increase in chamber temperature, evaporation of monomers in volatility bins $C^* = 10\text{--}100 \mu\text{g}/\text{m}^3$ and decomposition of oligomers lead to a decrease of the monomer and oligomer mass in the particle phase, respectively. As a result, the gas-phase dimers represent a greater fraction of the total condensed mass and their mass fraction increases from 22 % to 74 %.”*

In lines 365, the authors are comparing yields as a function of temperature with experiments from a prior publication (presumably under the same conditions and in the same chamber). It isn't clear that all of the kinetic processes are the same at 5 deg C as they are at 25 deg C. The rate constants (for oxidation, oligomerization, etc.) should have a dependence on temperature (as noted in the manuscript). Diffusion rates/viscosity may also be affected by the lower temperatures. Thus, unless everything is understood to be the same between this study and the Boyd study, it is misleading to state that the results are not in line with partitioning theory. It is more accurate to say that considering gas/particle partitioning alone, and the decrease in vapor pressure with temperature, higher SOA yields at lower temperatures would be expected.

Response: The referee is correct. We rephrased “which is not in line with equilibrium partitioning theory” to:

“This finding cannot be explained by gas-particle partitioning alone, as lower temperatures should give rise to higher SOA yields”.

We also added a sentence on oxidation chemistry:

Lines 376-378: *“A probable cause could be the temperature dependence of the gas phase oxidation chemistry, however, test calculations using the temperature-dependent rate coefficients reported in the MCM mechanism showed hardly any effect of temperature on SOA yield.”*

One of the things that is notably absent in the discussion of measured yields in this work, including comparisons with previously measured yields, is the role of gas-phase chemistry. The papers out of the Fry group (cited here and also Draper et al. ACP 2015) provide analysis of experimental monoterpene + NO₃ SOA data from a mechanistic perspective, and should be used here to strengthen the discussion regarding the measurement-model comparison (particularly lines 385-389).

Response: We agree that the role of gas-phase chemistry was not a focus of this manuscript. We rely on the lumped MCM mechanism that was presented earlier in Berkemeier et al. (2016) and we neither track individual gas phase products in the model nor in the experiment. Regardless, we added some general information from the model into the main text. Line numbers refer to the revised manuscript submitted with this comment.

We have discussed RO₂ fate in the original manuscript, e.g.:

Lines 429-431: *“The higher gas-phase dimer concentration can be explained by the higher initial precursor concentration used in the APN experiment that leads to a higher momentary RO₂ concentration (cf. Fig. S11) and hence a more pronounced RO₂ + RO₂ gas-phase chemistry compared to the LIM experiment.”*

We now added the following information on the branching coefficient to the revised manuscript:

Lines 431-433: *“The branching coefficient c_1 for dimer formation (cf. Fig. S3) is not included in the original MCM mechanism, but was determined here from the inverse modelling to be 1.96×10^{-2} .”*

Lines 311-312: *“Under the conditions employed in this study, limonene precursor oxidation is dominated by NO₃ oxidation. RO₂ fate is dominated by reaction with NO₃ and RO₂ as very little NO and HO₂ are present in the chamber.”*

Besides initial oxidation rates and RO₂ fate, this mechanism has limited effect on calculation results as the production ratio between nitrated and non-nitrated products can always be compensated with a different volatility distribution. We hint at this now in Sect. 3.4.

Lines 536-537: *“The model parameters that mainly determine pON/OA are the volatility distributions of the nitrated and non-nitrated oxidation products, but also the branching coefficients of the gas phase chemical mechanism (cf. Fig. S3).”*

A discussion of the determined branching coefficients themselves is now added to Sect. 3.4.

Lines 538-547: *“The chemical mechanism presented in this study deviates from the MCM template in that it allows nitrated alkoxy radicals (R^NO) to stabilize without elimination of the nitrate function. This is*

realized in the model using a branching coefficient c_4 that determines the fraction of $R^N O$ that loses its nitrate group during the conversion to a stable oxidation product. c_4 is determined to be 0 for the α -pinene system and 0.52 for the limonene system, both indicating a significant retrieval of stable organic nitrates from nitrated alkoxy radicals. A small value of c_4 stands in contrast to the findings of Kurtén et al. (2017) who ascribed the low organic nitrate yield in the oxidation of α -pinene with NO_3 to a predominant stabilization of $R^N O$ to the volatile and non-nitrated pinonaldehyde. Note that these calculations were performed at 25 °C, while α -pinene oxidation occurred at 5 °C in our experiments and model. c_4 itself is unlikely to have a positive temperature dependence, as the reaction pathway with the lower activation barrier should be even more favored at lower temperature. However, it may be possible that the fraction of alkyl radicals that undergo rearrangement (Vereecken et al., 2007) is enhanced at low temperature. The peroxy and alkoxy radicals resulting from such a rearrangement do not lose NO_2 upon stabilization. In addition, oxidation products with aldehyde moieties might be nitrated in a secondary reaction with NO_3 (Atkinson and Arey, 2003). This represents another channel of increasing pON/OA and is not considered in our model. Thus, the simple gas-phase chemistry branching coefficients c_2 - c_4 obtained through inverse modelling may be seen as effective parameters that represent gas-phase radical chemistry in the context of a certain experiment and volatility distribution, but their numerical values should not be evaluated in isolation.”

We also added this discussion to Sect. 5:

Lines 720-722: “However, the true parameter ranges can be much larger than apparent from these local sensitivity analyses. For example, changes in branching ratios in the gas phase chemical mechanism can in principle be offset with changes in the oxidation products' volatility distributions, thus forming a co-dependent parameter subset.”

We added a comparison of ΔH_{vap} for α -pinene oxidation products.

Lines 434-436: “The effective enthalpy of vaporization ΔH_{vap} of α -pinene oxidation products is determined to 81.3 kJ/mol, which is only slightly larger than values used in the SOA models ECHAM-HAM (59 kJ/mol; Saathoff et al., 2009), GEOS-Chem (42 kJ/mol; Chung and Seinfeld, 2002) or GISS-modeIE (72.9 kJ/mol; Tsigaridis et al., 2006).”

Lastly, we would like to point to some of the discussion of measured yields in the original manuscript, as well as comparisons with previously measured yields.

For limonene SOA:

Lines 296-299: “The produced aerosol mass corresponds to a SOA yield of 130 % (Table 2) and is observed to be constant in the chamber for several hours at 5 °C. Note that this observation is different from previous experiments conducted at 25 °C and 40 °C (Boyd et al. 2017), where peak aerosol mass was achieved swiftly and SOA yields at aerosol mass loadings similar to this study were determined to be 174 % and 94 %, respectively.”

For α -pinene SOA:

Lines 399-403: “The SOA yield in this study appears to be larger than previously reported for the oxidation of α -pinene with NO_3 : Hallquist et al. (1999) measured a 7 % yield (corresponding to 52.9 $\mu\text{g}/\text{m}^3$ organic aerosol) at 15 °C. Nah et al. (2016b) measured a yield of 3.6 % (corresponding to 2.4 $\mu\text{g}/\text{m}^3$ organic

aerosol) at room temperature. Fry et al. (2014) reported no significant aerosol growth at room temperature. This is indicative of the low temperature employed in the experiments having a significant impact on SOA yield.”

Are the oligomerization rates and product C* values consistent with those summarized in Barsanti et al. J. Phs. Chem. 2017?

Response: Thank you for mentioning this fitting compilation of important kinetic and thermodynamic data on accretion reactions. Barsanti et al. (2017) mention a hemiacetal formation rate in methanol under neutral conditions of $0.1 \text{ M}^{-1} \text{ h}^{-1}$ and a peroxyhemiacetal formation rate of $0.5\text{-}70 \text{ M}^{-1} \text{ h}^{-1}$. Assuming that every limonene oxidation product has two active sites to undergo hemiacetal formation, these rates correspond to first-order rates of $\sim 1 \text{ h}^{-1}$ and $5\text{-}700 \text{ h}^{-1}$, which are in the same ball park as our fit value of 17.2 h^{-1} . We added the following sentences to the manuscript.

Lines 332-337: *“Barsanti et al. (2017) compiled accretion rate coefficients with relevance to SOA formation and report rate coefficients for hemiacetal formation under neutral conditions in methanol of $0.1 \text{ M}^{-1} \text{ s}^{-1}$ and peroxyhemiacetal formation of $0.5\text{-}70 \text{ M}^{-1} \text{ s}^{-1}$. Assuming that every limonene oxidation product has two reactive sites to undergo oligomer formation, $k_{\text{form,lim}}$ can be translated into a second-order reaction rate coefficient of $1.4 \text{ M}^{-1} \text{ s}^{-1}$ and thus lies in close proximity to literature values.”*

Lines 340-342: *“Quantum chemical and mechanistic studies have previously predicted such pronounced differences between the volatility of typical oxidation products of monoterpenes and their oligomers of several orders of magnitude (DePalma et al., 2013;Barsanti et al., 2017).”*

In line 386, it is confusing to say that the yield is lower in the α -pinene experiment because more precursor was added. The yield is lower because α -pinene does not produce as much SOA as limonene under the same conditions, and thus to achieve the same mass loading for a compound with a lower yield, more precursor had to be added.

Response: We agree with the referee, this formulation is confusing, and correct it as follows:

Lines 394-398: *“Similar to the LIM experiment described above, oxidation at $5 \text{ }^\circ\text{C}$ initially causes a fast increase in aerosol mass (black open markers), however, peak aerosol mass is already reached after 3 hours of oxidation at $109 \mu\text{g}/\text{m}^3$ and a corresponding SOA yield of 25.2 % (Table 2). At a comparable organic mass, this yield is significantly lower than observed in the limonene oxidation experiment. Note that, in order to achieve similar aerosol mass loadings among all experiments in this study, a larger amount of precursor is added in the α -pinene oxidation experiment.”*

Editorial comments:

43: “sink” should be “sinks”

Response: Thank you, this has been changed.

60: The latter "...is missing completely..." is repetitive; suggest to remove that part of the sentence.

Response: We adopted this good suggestion.

83: "allows to infer" should be "allows inference of"

Response: We adopted this good suggestion.

96: "pinene" in "alpha-" should be capitalized

Response: Thank you, well spotted.

141-142: Description of sequential precursor oxidation experiments is awkward and unclear as written; needs revision.

Response:

257: "residue" should be "residual"

Response: Thank you, this has been changed.

321: the second "non-nitrated" should be "nitrated"

Response: Precisely, thank you very much.

343: "constant drift" suggests a physical process, and not a chemical thermodynamics process

Response: The chemical process we are referring to here is the oligomer formation & decomposition equilibrium. Removal of monomers (through the physical process of evaporation) induces a net flux of reactants towards the monomer side of the chemical equation. We agree that the word "drift" was meant rather figuratively here and is potentially misleading. We suggest to change "constant drift" into "constant flux".

Figure S4: This figure was difficult for me to understand. I did not see what it added to the paper.

Response: The referee is right. Fig. S4 was removed from the manuscript.

Figure S5: This figure is confusing as labeled. The insets are labeled “SOA”, but the volatility distributions clearly include products that reside only in the gas-phase.

Response: We agree, please excuse this inaccuracy. The labels now match the caption and read “oxidation products” instead of “SOA” in what is now Fig. S4.

Figure S6: There is a mismatch between the legend and the traces (black line appears to be total).

Response: Thank you, well spotted.

References

- Atkinson, R., and Arey, J.: Atmospheric Degradation of Volatile Organic Compounds, *Chemical Reviews*, 103, 4605-4638, 10.1021/cr0206420, 2003.
- Barsanti, K. C., Kroll, J. H., and Thornton, J. A.: Formation of Low-Volatility Organic Compounds in the Atmosphere: Recent Advancements and Insights, *The Journal of Physical Chemistry Letters*, 8, 1503-1511, 10.1021/acs.jpcllett.6b02969, 2017.
- Berkemeier, T., Ammann, M., Mentel, T. F., Pöschl, U., and Shiraiwa, M.: Organic Nitrate Contribution to New Particle Formation and Growth in Secondary Organic Aerosols from α -Pinene Ozonolysis, *Environmental Science & Technology*, 50, 6334-6342, 10.1021/acs.est.6b00961, 2016.
- DePalma, J. W., Horan, A. J., Hall Iv, W. A., and Johnston, M. V.: Thermodynamics of oligomer formation: implications for secondary organic aerosol formation and reactivity, *Physical Chemistry Chemical Physics*, 15, 6935-6944, 10.1039/C3CP44586K, 2013.
- Kurtén, T., Møller, K. H., Nguyen, T. B., Schwantes, R. H., Misztal, P. K., Su, L., Wennberg, P. O., Fry, J. L., and Kjaergaard, H. G.: Alkoxy Radical Bond Scissions Explain the Anomalously Low Secondary Organic Aerosol and Organonitrate Yields From α -Pinene + NO₃, *The Journal of Physical Chemistry Letters*, 8, 2826-2834, 10.1021/acs.jpcllett.7b01038, 2017.
- Nah, T., McVay, R. C., Zhang, X., Boyd, C. M., Seinfeld, J. H., and Ng, N. L.: Influence of seed aerosol surface area and oxidation rate on vapor wall deposition and SOA mass yields: a case study with α -pinene ozonolysis, *Atmos. Chem. Phys.*, 16, 9361-9379, 10.5194/acp-16-9361-2016, 2016a.
- Nah, T., Sanchez, J., Boyd, C. M., and Ng, N. L.: Photochemical Aging of α -pinene and β -pinene Secondary Organic Aerosol formed from Nitrate Radical Oxidation, *Environmental Science & Technology*, 50, 222-231, 10.1021/acs.est.5b04594, 2016b.
- Vereecken, L., Müller, J. F., and Peeters, J.: Low-volatility poly-oxygenates in the OH-initiated atmospheric oxidation of α -pinene: impact of non-traditional peroxy radical chemistry, *Physical Chemistry Chemical Physics*, 9, 5241-5248, 10.1039/B708023A, 2007.

Kinetic modelling of formation and evaporation of SOA from NO₃ oxidation of pure and mixed monoterpenes

Thomas Berkemeier^{1,2}, Masayuki Takeuchi³, Gamze Eris⁴, and Nga L. Ng^{1,4}

¹School of Chemical and Biomolecular Engineering, Georgia Institute of Technology, Atlanta, GA, USA

²Multiphase Chemistry Department, Max Planck Institute for Chemistry, Mainz, Germany

³School of Civil and Environmental Engineering, Georgia Institute of Technology, Atlanta, GA, USA

⁴School of Earth and Atmospheric Sciences, Georgia Institute of Technology, Atlanta, GA, USA

Correspondence: Thomas Berkemeier (t.berkemeier@mpic.de) and Nga Lee Ng (ng@chbe.gatech.edu)

Abstract.

Organic aerosol constitutes a major fraction of the global aerosol burden and is predominantly formed as secondary organic aerosol (SOA). Environmental chambers have been used extensively to study aerosol formation and evolution under controlled conditions similar to the atmosphere, but quantitative prediction of the outcome of these experiments is generally not achieved, which signifies our lack in understanding of these results and limits their portability to large scale models. In general, kinetic models employing state-of-the-art explicit chemical mechanisms fail to describe the mass concentration and composition of SOA obtained from chamber experiments. Specifically, chemical reactions including the nitrate radical (NO₃) are a source of major uncertainty for assessing the chemical and physical properties of oxidation products. Here, we introduce a kinetic model that treats gas-phase chemistry, gas-particle partitioning, particle-phase oligomerization and chamber vapor wall loss and use it to describe the oxidation of the monoterpenes α -pinene and limonene with NO₃. The model can reproduce aerosol mass and nitration degrees in experiments using either pure precursors or their mixtures and infers volatility distributions of products, branching ratios of reactive intermediates as well as particle-phase reaction rates. The gas-phase chemistry in the model is based on the Master Chemical Mechanism (MCM), but trades speciation of single compounds for the overall ability of quantitatively describing SOA formation by using a lumped chemical mechanism. The complex branching into a multitude of individual products in MCM is replaced in this model with product volatility distributions, detailed peroxy (RO₂) and alkoxy (RO) radical chemistry and amended by a particle-phase oligomerization scheme. The kinetic parameters obtained in this study are constrained by a set of SOA formation and evaporation experiments conducted in the Georgia Tech Environmental Chamber (GTEC) facility. For both precursors, we present volatility distributions of nitrated and non-nitrated reaction products that are obtained by fitting the kinetic model systematically to the experimental data using a global optimization method, the Monte Carlo Genetic Algorithm (MCGA). The results presented here provide new mechanistic insight into the processes leading to formation and evaporation of SOA. Most notably, the model suggests that the observed slow evaporation of SOA could be due to reversible oligomerization reactions in the particle phase. However, the observed non-linear behavior of precursor mixtures points towards a complex interplay of reversible oligomerization and kinetic limitations of mass transport in the particle phase, which is explored in a model sensitivity study. The methodologies described in this work provide a basis for quantitative

25 analysis of multi-source data from environmental chamber experiments, but also show that a large data pool is needed to fully
resolve uncertainties in model parameters.

1 Introduction

Atmospheric aerosol particles play an important role in the Earth system by influencing weather and climate, enabling long-
range transport of chemical compounds and negatively affecting public health (Pöschl, 2005; Fuzzi et al., 2006). A major
30 contributor to the global aerosol burden is the oxidation of volatile organic compounds (VOCs) to condensable organic species,
which leads to formation of secondary organic aerosol (SOA; Kanakidou et al., 2005). Important classes of SOA precursors
include alkanes and aromatic compounds, which are often emitted from anthropogenic sources, as well as alkenes such as iso-
prene, monoterpenes, and sesquiterpenes, which are predominantly emitted by trees (Hallquist et al., 2009). The monoterpenes
 α -pinene and limonene are among the most abundant and well-studied SOA precursors (Seinfeld and Pandis, 2016). Atmo-
35 spheric oxidation of alkenes occurs mainly through three oxidants: the hydroxyl radical (OH), which is produced in daylight
and is short-lived; the abundant, but comparatively slow reacting ozone (O_3); and the nitrate radical (NO_3), which is the major
source of SOA at nighttime, but also contributes to SOA formation during daytime, despite its quick photolysis (Liebmann
et al., 2019). The oxidation of VOCs by NO_3 results in the formation of high yields of various nitrated organic compounds,
alkyl nitrates and peroxy acyl nitrates, which are produced in lower quantities through other atmospheric oxidation channels
40 such as reaction of organic peroxy radicals (RO_2) or hydroperoxy radicals (HO_2) with nitric oxide (NO) (Perring et al., 2013;
Ng et al., 2017). These organic nitrates (ON) play an important role in the atmospheric nitrogen budget by serving as temporary
or permanent sinks for highly reactive nitrogen oxides ($NO_x = NO + NO_2$).

Due to their sufficiently low volatility, ON can be taken up into atmospheric aerosol particles, where they are shielded
from gas-phase chemical decomposition, causing NO_x to be temporarily removed from atmospheric oxidation cycling. While
45 NO_x can be recycled back into the atmosphere via photolysis (Müller et al., 2014), photooxidation (Nah et al., 2016b), and
thermal decomposition of ON, permanent removal can occur through ON hydrolysis (Takeuchi and Ng, 2019) and deposition
processes (Nguyen et al., 2015).

Furthermore, the presence of ON affects the formation and persistence of organic aerosol (OA) (Ng et al., 2017). The
contribution of particulate ON mass (pON) to total organic aerosol (pON/OA) has been investigated previously in laboratory
50 studies by mass-spectrometric methods (Fry et al., 2009, 2011, 2014; Boyd et al., 2015; Nah et al., 2016b; Boyd et al., 2017;
Faxon et al., 2018; Takeuchi and Ng, 2019) and a radioactive tracer method (Berkemeier et al., 2016), revealing that pON/OA
can reach up to 0.9 in the particle phase under certain conditions. Although ambient pON/OA varies strongly temporally and
regionally, measured values of the ratio of organic mass in ON to the total organic mass have been shown to reach up to
0.77 (Ng et al., 2017, and references therein).

55 Despite the importance of ON to the dynamics of SOA formation, the chemical mechanism for their formation in the
gas and particle phases is still under discussion (Kurtén et al., 2017; Claffin and Ziemann, 2018; Draper et al., 2019). The
Master Chemical Mechanism (MCM) provides a resource of the gas phase degradation chemistry of typical SOA precursors

with atmospheric oxidants (Saunders et al., 2003; Jenkin et al., 2003). However, application of MCM to the oxidation of monoterpenes with NO₃ leads to a significant underestimation of particle mass and pON/OA as this mechanism is missing several important chemical reactions, for example, oxidation of the second double bond of limonene (Boyd et al., 2017; Faxon et al., 2018).

It has been hypothesized and shown recently that a majority of SOA might exist in oligomerized form (Kalberer et al., 2004; Gao et al., 2010), which might alter their evaporation behavior (Baltensperger et al., 2005; D'Ambro et al., 2018). In that case, the evaporation time scale is determined by chemical decomposition instead of equilibrium partitioning due to volatility (Pankow, 1994). Additionally, organic aerosol particles can exhibit a highly viscous phase state (Virtanen et al., 2010; Koop et al., 2011; Reid et al., 2018), which leads to kinetic limitations in evaporation (Vaden et al., 2011), slowing of particle-phase chemistry (Gatzsche et al., 2017), and non-equilibrium partitioning (Cappa and Wilson, 2011).

To describe kinetic limitations in mass transport, a number of kinetic multi-layer models have been developed recently to describe aerosol particles and cloud droplets, including KM-SUB (Shiraiwa et al., 2010), KM-GAP (Shiraiwa et al., 2012), ADCHAM (Roldin et al., 2014), and MOSAIC (Zaveri et al., 2008, 2014). These models are capable of explicitly resolving mass transport and chemical reactions within aerosol particles. Using these models, Shiraiwa et al. (2013) and Zaveri et al. (2018) were able to find evidence for diffusion limitation affecting SOA formation dynamics by inspection of the evolution of particle size distributions. Yli-Juuti et al. (2017) and Tikkanen et al. (2019) used an evaporation model based on KM-GAP to describe the interaction of volatility and viscosity during isothermal dilution as a function of different environmental conditions. However, to the best of our knowledge, no model has been presented that describes all aspects of gas-phase chemistry, particle-phase chemistry, gas-particle partitioning and bulk diffusion of SOA.

A model capable of describing all these aspects of SOA formation must rely on a large set of kinetic parameters, which are often not readily accessible. However, model parameters can be systematically altered so the model matches experimental data, an approach often referred to as inverse modelling. Simultaneously optimizing multiple model parameters can often be unfeasible via manual optimization and prompts the use of global optimization methods (Berkemeier et al., 2013, 2017). As opposed to local optimization methods, global optimization algorithms are not as easily stuck in local minima and are able to reliably find solutions of difficult optimization problems. In conjunction with a kinetic model, global optimization algorithms represent a powerful tool that allows **inference of** molecular level information from macroscopic data. Thus, global optimization algorithms based on differential evolution, such as the Monte Carlo Genetic Algorithm (MCGA), have become increasingly popular in the modelling of complex multiphase chemical systems (Berkemeier et al., 2017; Marshall et al., 2018; Tikkanen et al., 2019).

In a previous study, Boyd et al. (2017) showed that the retained aerosol mass from oxidation of limonene with NO₃ after heating from 25 °C to 40 °C is significantly different than the mass obtained from oxidizing limonene at 40 °C. They further showed that the evaporation behavior of mixtures of limonene SOA and β -pinene SOA crucially depends on the order in which oxidation occurred. Oxidation of limonene followed by subsequent oxidation of β -pinene led to an aerosol that exhibits much slower evaporation of limonene compared to an aerosol produced by simultaneous oxidation of the two precursors. At the time, it was only postulated that diffusion limitations and/or oligomerization reactions could have led to these observations. In

this work, we conduct new environmental chamber experiments and apply a novel kinetic modelling framework to investigate whether gas-phase chemistry, equilibrium partitioning, and particle-phase chemistry can accurately describe the formation and evaporation of monoterpene SOA from oxidation of α -pinene, limonene, and mixtures of both precursors with NO_3 . α -Pinene is chosen over β -pinene since it shows a more distinct evaporation behavior to limonene SOA and is the overall better-understood SOA precursor. We perform experiments at a lower initial temperature compared to Boyd et al. (2017) to include a second heating stage in the experiments. We focus the modelling efforts on the experimental observables aerosol mass and organic nitrogen content (pON/OA) as a function of time in the reaction chamber. The model uses a simplified, lumped kinetic mechanism based on MCM (Berkemeier et al., 2016), but modifies some of the branching ratios in RO_2 chemistry and adds chemical reactivity in the particle phase. Building on the observations of Boyd et al. (2017) in their mixed precursor experiments, we investigate the linearity of these two observables by quantitative comparison of formation and evaporation of SOA from pure and mixed monoterpene precursors. We first test the hypothesis whether particle-phase oligomerization in a well-mixed liquid phase can explain the observed behavior. Then, we use the kinetic model to perform a sensitivity analysis on the potential effect of retarded bulk diffusion due to a viscous phase state. The kinetic modelling framework consisting of a kinetic multi-layer model based on KM-GAP and the MCGA algorithm is used as analysis tool to explore the mechanistic interactions between reactive intermediates and oxidation products that can lead to non-additivity of the investigated reaction systems.

2 Experimental and theoretical methods

2.1 Georgia Tech environmental chamber (GTEC)

The aerosol formation and evaporation experiments are performed as batch reactions in the GTEC facility, which consists of two separate 12 m^3 Teflon chambers in a temperature- and humidity-controlled enclosure (Boyd et al., 2015). A consistent experimental routine is maintained for all experiments presented in this study and resembles the method used by Boyd et al. (2017) with small updates. Concentrations of O_3 and NO_x are determined with a UV absorption O_3 analyzer (Teledyne T400) and a chemiluminescence NO_x monitor (Teledyne 200 EU), respectively. Aerosol particle number and volume concentrations are measured using a scanning mobility particle sizer (SMPS, TSI), which consists of a differential mobility analyzer (DMA, TSI 3040) and a condensation particle counter (CPC, TSI 3775). Bulk aerosol composition is measured using a High Resolution Time-of-Flight Aerosol Mass Spectrometer (HR-ToF-AMS, DeCarlo et al., 2006).

The Teflon chamber is flushed with zero air for at least 24 h and the chamber enclosure is cooled to $5 \text{ }^\circ\text{C}$ several hours prior to each experiment, to ensure full equilibration with regard to temperature, pressure, and humidity. Monoterpene oxidation is initiated at $5 \text{ }^\circ\text{C}$ and under dry conditions ($\text{RH} < 5 \%$). All experiments are conducted using ammonium sulfate seed particles. Seed particles are generated by atomizing a 15 mM ammonium sulfate solution into the chamber for 20 minutes, which typically results in particle number concentrations around $20\,000 \text{ cm}^{-3}$ and mass concentrations of $28 - 41 \text{ } \mu\text{g}/\text{m}^3$. Simultaneously, monoterpene precursors are injected into the chamber. Injection volumes of the precursors are chosen to achieve consistent total aerosol mass concentrations around $100 \text{ } \mu\text{g}/\text{m}^3$ in all experiments, based on knowledge about aerosol yields in

trial experiments for this study. For α -pinene, we use a micro syringe to inject a known volume of liquid into a mildly heated glass bulb from which a 5 L/min zero air flow carries the evaporating fumes into the chamber. For limonene, the required liquid volume is so low that the use of micro syringes is a source of non-negligible uncertainty and hence a gas cylinder filled with 0.85 ppm limonene, calibrated and confirmed using gas chromatography with flame ionization detection (GC-FID), is used to inject a known volume of gas into the chamber over the course of several minutes. NO_3 is produced by oxidation of NO_2 with O_3 (generated by passing zero air through a photochemical ozone generator) in a 1.5 L flow tube (0.9 L/min flow, 100 s residence time). The reaction mixture is optimized so NO_3 and N_2O_5 are produced in high yields, with no significant amount of O_3 entering the chamber. This is achieved by using a 2:1 ratio of NO_2 and O_3 . N_2O_5 decomposes in the chamber to release NO_3 over time. Injection of $\text{NO}_3/\text{N}_2\text{O}_5$ marks the beginning of the reaction.

When peak SOA mass is reached, which is typically achieved in under 4 hours, the chamber enclosure temperature is raised to 25 °C and, after another waiting period, to 42 °C. The temperature changes take approximately 90 minutes in both cases. Temperature profiles are reported alongside the experimental results in Fig. 2.

In total, four experiments are conducted, either with a single monoterpene precursor, pure α -pinene (APN) and pure limonene (LIM), or with a mixture of both precursors. In the case where both precursors are used, the oxidation occurred in one of two variants: simultaneous (MIX) or sequential oxidation (SEQ). In case of the MIX experiment, both precursors are injected simultaneously into the chamber prior to $\text{NO}_3/\text{N}_2\text{O}_5$ injection. In case of the SEQ experiment, peak SOA mass after the first precursor oxidation is first awaited. Then, a second $\text{NO}_3/\text{N}_2\text{O}_5$ injection and injection of the second VOC follow in sequence. An 8-fold excess of N_2O_5 is used for pure limonene experiments, and a 4-fold excess used for pure α -pinene experiments. In the mixed precursor experiments, the amount of injected $\text{NO}_3/\text{N}_2\text{O}_5$ is determined using the same ratios proportionately. A summary of all experimental conditions, including injected precursor amounts, **seed mass**, **total aerosol mass**, organic aerosol mass excluding seed, and SOA yields can be found in Table 1. It is noted that we refer to the total aerosol mass concentration (sum of inorganic seed mass concentration and organic aerosol mass concentration) in the chamber simply as “aerosol mass” in our discussions. We use the term “SOA yield” to refer to the ratio of produced organic aerosol mass concentration to the initial VOC mass concentration.

2.2 Kinetic model

The kinetic model calculations in this study are performed with a multi-compartmental model akin to the KM-SUB/KM-GAP model family (Shiraiwa et al., 2010, 2012). The model code is set up as a generator script that uses an input chemical mechanism to generate a system of differential equations that is able to describe the key physical and chemical processes in the GTEC chamber. The model compartments include the chamber wall, the wall near-surface gas phase, the chamber gas phase, the particle near-surface gas phase, the particle surface, and the particle bulk. The processes explicitly described in the model include injection of chemical compounds, irreversible loss of wall-adsorbed species, temperature change, gas diffusion to the chamber wall, gas diffusion to particles, condensation and evaporation at the wall and particle surfaces, as well as chemical reactions in the gas and particle phases. Wall loss of particles is implicitly accounted for in this study by using wall loss-corrected SMPS data (Keywood et al., 2004; Nah et al., 2017).

160 All product molecules with vapor pressures lower than 1 Pa at 298 K are allowed to partition into the topmost layer of the particles, according to their volatility. Gas-particle partitioning is explicitly treated in the model and equilibration between the particle near-surface gas phase and the particle surface is achieved by balancing surface adsorption and desorption rates. This way, evaporation and condensation kinetics are treated more realistically than in a model assuming instantaneous equilibrium partitioning. The adsorption flux $J_{\text{ads},X}$ of a molecule X is calculated from the collision flux from the particle near-surface gas phase to the particle surface, which in turn is calculated from the mean thermal velocity ω_X and the accommodation coefficient $\alpha_{\text{s},X}$. $\alpha_{\text{s},X}$ is assumed to be 0.5 for all organic species in this study, in line with previous investigations (Julin et al., 2013; von Domaros et al., 2020). A sensitivity study on the effect of $\alpha_{\text{s},X}$ on model output can be found in Fig. S1 in the Supplement.

$$J_{\text{ads},X} = \alpha_{\text{s},X} \cdot \frac{\omega_X}{4} \cdot [X]_{\text{gs}} \quad (1)$$

170 The desorption flux from the particle surface to the gas phase $J_{\text{des},X}$ is dependent on the vapor pressure $p_{\text{vap},X}$ and the ratio of the concentration of X in the particle near-surface bulk layer $[X]_{\text{b1}}$ (in unit cm^{-3}) and the sum of all other species Y_j in that layer.

$$J_{\text{des},X} = \frac{\alpha_{\text{s},X} \cdot \omega_X \cdot p_{\text{vap},X} \cdot N_{\text{A}} \cdot [X]_{\text{b1}}}{4 \cdot R \cdot T \cdot \sum [Y_j]_{\text{b1}}} \quad (2)$$

175 Here, R is the universal gas constant, T the temperature in K, and N_{A} is Avogadro's number. The vapor pressure of product compounds is assumed to be temperature dependent with a precursor-dependent effective enthalpy of volatilization, $\Delta H_{\text{vap},Z}$ in kJ/mol, where Z is the precursor of X . We assume this single effective enthalpy to be representative for the entire product spectrum and hence independent of C^* .

$$p_{\text{vap},X}(T) = p_{\text{vap},X}(298 \text{ K}) \cdot \exp \frac{-\Delta H_{\text{vap},Z}}{R \cdot (T - 298)} \quad (3)$$

180 Note that, while the employed model is inherently a multi-layer model, only a single well-mixed layer is used to describe the aerosol phase in the default calculations in this study. Multiple layers were used for the calculations in Sect. 3.5.3 leading to Fig. 6. New particle formation from low-volatility vapors is not treated in this model, so seed particles have to be pre-defined. Seed particles are initialized as covered with a very small amount of non-volatile organics (5×10^{-3} ppb gas phase mixing ratio) to aid in computation of gas-particle partitioning. The model can be run in two modes: lumped mode, in which only vapor pressure bins are defined, and explicit mode, in which vapor pressures must be pre-supplied for all participating species. In the following, we will describe the specific lumped mode used in this study.

185 Reversible and irreversible vapor wall loss is described following Huang et al. (2018) with slight modifications to fit into the KM-SUB/KM-GAP model structure. The Teflon wall is described using two layers: a surface layer, to which vapor molecules partition reversibly, and an inner layer, into which vapor molecules diffuse irreversibly on the time scale of the experiment. The wall adsorption flux $J_{\text{ads},X,\text{wall}}$ is parameterized according to Eq. (4).

$$J_{\text{ads},X,\text{wall}} = \alpha_{\text{wall}} \cdot \frac{\omega_X}{4} \cdot [X]_{\text{ws}} \quad (4)$$

190 $[X]_{\text{ws}}$ is the wall near-surface gas phase concentration of X . The wall accommodation coefficient $\alpha_{\text{wall},X}$ is parameterized according to Eq. (5).

$$\alpha_{\text{wall},X} = 10^{-2.744} \cdot C_X^{*-0.6566} \quad (5)$$

C_X^* is the saturation mass concentration of X , which indicates the organic aerosol mass at which a semi-volatile organic substance would be in the gas and particle phase in equal parts. The wall desorption flux $J_{\text{des},X,\text{wall}}$ is parameterized according to Eq. (6).

$$J_{\text{des},X,\text{wall}} = \alpha_{\text{wall}} \cdot \frac{\omega_X}{4} \cdot \frac{\gamma^\infty C_X^* M_{\text{W,wall}}}{10^3 C_{\text{wall}} M_{\text{W},X}} \quad (6)$$

Here, γ^∞ is the activity coefficient in Teflon and C_{wall} the effective organic mass concentration of the wall itself and is set to be 32.2 mg m^{-3} (Huang et al., 2018). $M_{\text{W},X}$ and $M_{\text{W,wall}}$ denote the molecular weight of X and the effective molecular weight of the Teflon wall, respectively.

$$200 \quad \gamma^\infty = 10^{3.299} \cdot C_X^{*-0.6407} \quad (7)$$

The gas diffusion flux from the chamber interior to the wall near-surface gas phase $J_{\text{dif},X,\text{ws}}$ is described using the Fickian gas diffusivity coefficient $D_{g,X}$ and an additional Eddy diffusivity coefficient k_e , which was estimated to be 0.03 s^{-1} for the GTEC chamber in a previous study (Nah et al., 2016a).

$$J_{\text{dif},X,\text{ws}} = \frac{2}{\pi i} \sqrt{D_{g,X} k_e} [X]_{\text{g}} \quad (8)$$

205 Note that the explicit treatment of a near-surface gas phase at the wall constitutes a slight variation from the framework of Huang et al. (2018), who treated gas diffusion and adsorption simultaneously in a resistor-style approach. The two resistor terms were split into the separate fluxes $J_{\text{ads},X,\text{wall}}$ and $J_{\text{dif},X,\text{ws}}$ in this study. The thickness of the near-wall gas phase had only little impact on calculation results in the range of 0.1 mm - 1 cm and was set to the higher limit of 1 cm for numerical stability. Irreversible transport from the Teflon surface layer to the inner Teflon layer is assumed to occur at a first-order rate $l_{\text{w},i}$, and treated as independent of volatility of the organic molecule. $l_{\text{w},i}$ is obtained by fitting the model to experimental data and typically falls around 10^{-4} s^{-1} or 0.3 h^{-1} (cf. Table 1).

2.3 Lumped chemical mechanism

The gas-phase chemical mechanism, summarized in Fig. 1a, is modeled after the initial reaction steps in the MCM, but does not assume specific sum or structural formulas of product molecules. The validity of this approach has been shown in previous work (Berkemeier et al., 2016). For limonene SOA, we apply the same general chemistry, but consider the oxidation of both double bonds individually, which leads to the more complex reaction scheme shown in Fig. S2. Note that oxidation of the second double bond of limonene with NO_3 is not considered in MCM. However, we have shown previously that including oxidation of the second double bond leads to a significantly improved correlation between a kinetic model and chamber experiments (Boyd et al., 2017).

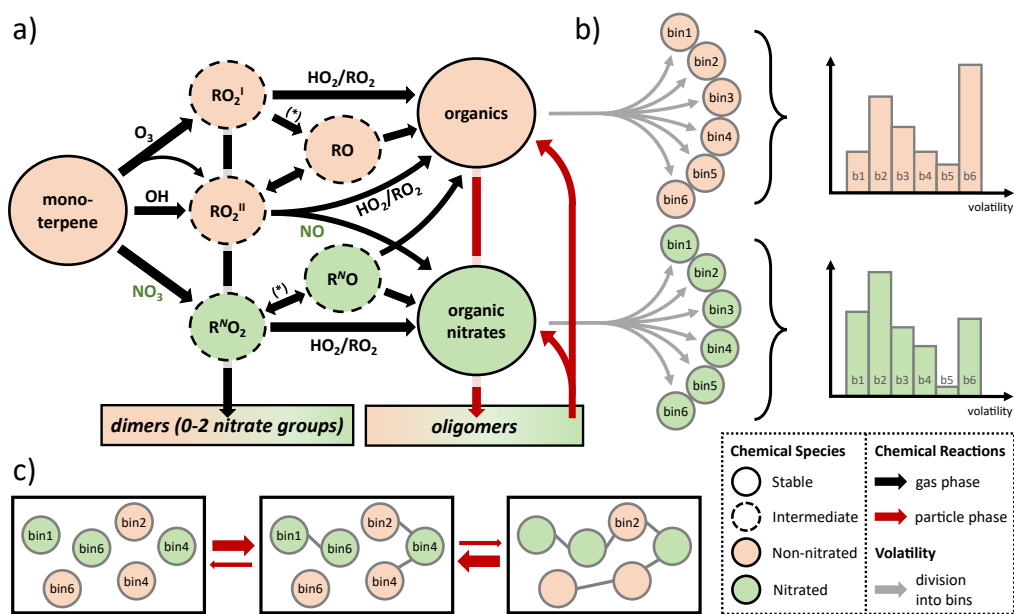


Figure 1. (a) Schematic representation of the lumped chemical mechanism for oxidation of monoterpenes with one double bond (e.g., α -pinene). The asterisk stands for chemical reaction with NO, NO₃, and RO₂. (b) The stable products are divided into 6 product bins each with a different volatility (grey arrows; bin1-bin6), according to a probability distribution (exemplary graphs on the right). (c) Oligomerization occurs in equilibrium reactions in the particle phase under conservation of precursor origin and volatility bin.

220 To account for chemical identity, the major product classes, nitrated and non-nitrated organic molecules, are subdivided into logarithmically-spaced volatility bins (Fig. 1b) following the concept of a volatility basis set (VBS; Donahue et al., 2011). To minimize the number of model parameters, six volatility bins are chosen with higher resolution in and around the experimental range (1 – 1000 $\mu\text{g}/\text{m}^3$) to achieve high sensitivity. To also cover a wide range of volatilities, a very low volatility and a very high volatility bin are included at the ends of the spectrum: (1) 9.91×10^{-8} Pa ($C^* = 0.01 \mu\text{g}/\text{m}^3$), (2) 9.91×10^{-6} Pa
 225 ($C^* = 1 \mu\text{g}/\text{m}^3$), (3) 9.91×10^{-5} Pa ($C^* = 10 \mu\text{g}/\text{m}^3$), (4) 9.91×10^{-4} Pa ($C^* = 100 \mu\text{g}/\text{m}^3$), (5) 9.91×10^{-3} Pa ($C^* = 1000 \mu\text{g}/\text{m}^3$) and (6) 9.91×10^{-1} Pa ($C^* = 100\,000 \mu\text{g}/\text{m}^3$) at 298 K. Oligomeric species are chosen to be fully non-volatile and hence technically form a seventh volatility bin. The average molar mass of molecules in the organic aerosol phase is assumed to be 250 g/mol, which is similar to assumptions in previous publications (Berkemeier et al., 2016) and consistent with our measurements using chemical ionization high-resolution time-of-flight mass spectrometry with a special filter inlet that
 230 samples both the aerosol and gas phase (FIGAERO-HRToF-CIMS Lopez-Hilfiker et al., 2014) that were conducted alongside this study (Takeuchi and Ng, 2019).

A specific aim of this study is the mechanistic analysis of ON formation. Therefore, the gas-phase formation of ON is treated in detail and has been expanded from the MCM template, which is detailed in Fig. S3. We assume that chemical reaction of NO₃ with the terpenic precursor yields a nitrated peroxy radical (R^NO₂). The fate of the nitrate group (-ONO₂) in this radical

235 is dependent on its radical branching ratios. Following MCM, we assume that the reaction of $R^N O_2$ with HO_2 yields a stable organic nitrate product, whereas reaction with NO , NO_3 , RO_2 , or unimolecular decay leads to formation of a nitrated alkoxy radical ($R^N O$), which can further stabilize under elimination of the nitrate group. Reaction of two RO_2 may also yield dimers. Another channel of ON formation is the reaction of a non-nitrated peroxy radical (RO_2^I) with NO . Following MCM, we assume that only RO_2^II , which is the main intermediate in monoterpene OH oxidation and a secondary intermediate of monoterpene
240 ozonolysis, can undergo this reaction and is in that regard distinct from RO_2^I , which is the main intermediate in monoterpene ozonolysis. However, this $RO_2^II + NO$ reaction channel has only minor implications in this study due to the low prevalence of NO under the employed reaction conditions, i.e., injection of NO_3/N_2O_5 as well as no irradiance with UV lights.

Particle-phase chemistry is included as formation and decomposition of oligomers from monoterpene oxidation products. Possible reaction pathways for oligomerization include the formation of esters, aldols, hemiacetals, acetals, peroxyhemiac-
245 etals, and peroxyacetals from alcohol, aldehyde, hydroperoxide, and carboxylic acid moieties in the monoterpene oxidation products (Ziemann and Atkinson, 2012), but are lumped into a single reaction for simplicity. These oligomers are assumed to be non-volatile, which is in line with recent investigations (DePalma et al., 2013; Barsanti et al., 2017), but can re-partition back to the gas phase after decomposition into the monomeric building blocks. Oligomer decomposition is treated as temperature dependent with a precursor-specific activation energy $E_{A,decom,Z}$ of precursor Z to be used in an Arrhenius equation.
250 The information about volatility and nitration degree of monomers is retained during oligomerization and reinstated after their decomposition. This process is outlined in Fig. 1c. A discussion of the oligomerization scheme is provided in the Supplement, Sect. S1. An overview of all reactions of the lumped model in the gas and particle phases is given in Table S1.

2.4 Global optimization

The Monte Carlo Genetic Algorithm (MCGA; Berkemeier et al., 2017) is applied for inverse fitting of the kinetic model to
255 the experimental data and determining the non-prescribed kinetic parameters listed in Table 1. The MCGA method consists of two steps: a Monte Carlo step and a genetic algorithm step. During the Monte Carlo step, kinetic parameter sets are randomly sampled from a defined parameter range and the residual between the model result and the experimental data is determined for each parameter set through evaluation of the kinetic model. During the genetic algorithm step, the parameter sets are optimized mimicking processes known from natural evolution: a survival mechanism retains best-fitting parameter sets, the
260 recombination mechanic generates new parameter sets by combing parameters of high scoring sets, and the mutation step prevents early homogenization of the sample of parameter sets. To determine the model-experiment correlation, we use a least-squares approach that minimizes the sum of the squares of the residuals, Eq. 9. The estimator is normalized to the magnitude of the largest data point in a given sample, $\max(Y_i)$, and the number of data points n_i of data set i . Additionally, optional weighting factors w_i can be used to guide the optimization process. In this study, pure precursor experiments are each
265 weighted twice as high as the mixed precursor experiments to ensure that any non-linearity in the mixed precursor experiments is detected as a deviation between model and experiment for those experiments. pON/OA data is weighted by a factor of 4 less than SOA mass data as the focus of this paper is the formation and evaporation behavior of SOA and more assumptions go into

the determination of pON/OA.

$$f_i = w_i \sqrt{\frac{1}{n_i} \sum \left(\frac{Y_{\text{model}} - Y_{\text{data},i}}{\max(Y_{\text{data},i})} \right)^2} \quad (9)$$

270 After an optimization result is returned, a 1-dimensional golden-section search (Press et al., 2007, Sect. 10.2) is used to ensure conversion into a minimum of the optimization hypersurface. The simplex method (Press et al., 2007, Sect. 10.5) is used to find other combinations of parameters that lead to equivalent model results (test of uniqueness). Weighting factors w_i can be used to assign a lower importance to data sets that e.g., exhibit large scatter due to experimental noise, represent experimental artifacts or are deemed only supplementary for the purpose of the optimization.

275 Note that for the experiments discussed in this manuscript, multiple model solutions can be obtained, dependent not only on the choice of data sets that is optimized to, but also on the choice of weighting factors. In the following sections, we focus our discussion on one fit of the model to experimental data as it scored best in our choice of model-experiment correlation estimator ("fit 1", $f = 0.88$ according to Eq. 9). Multiple evaluations of MCGA typically give similar results to fit 1, but sometimes get stuck in local minima that are significantly worse. This is a direct consequence of undersampling with MCGA, given the large
280 amount of model input parameters. Typically, about 150000 parameter sets were sampled during a MCGA run, which is not sufficient given the number of input parameters, but marks an upper achievable range for this study as it takes about three days to complete on an 80 CPU computer cluster. Among the inferior fits that were obtained, we also found a distinct fit that scores worse overall ("fit 2", $f = 0.097$), but scores better in some aspects of the data set and will be discussed alongside fit 1. We will discuss the dependence of the best fit on weighting factors and the uniqueness of the obtained model solution in Sects. 3.5
285 and 4.

3 Results and discussion

3.1 Pure limonene oxidation (LIM)

3.1.1 Experimental observations (LIM)

Fig. 2a shows the total aerosol mass concentration (denoted as "aerosol mass") during an experiment of limonene oxidation
290 with NO_3 in the presence of ammonium sulfate seed particles, and subsequent evaporation in the GTEC chamber, here referred to as "LIM" experiment. Oxidation at 5 °C initially causes a fast increase in aerosol mass (black open markers, left axis) from 29 $\mu\text{g}/\text{m}^3$ of seed mass to about 70 $\mu\text{g}/\text{m}^3$ of aerosol mass within the first 20 minutes of the experiment. Afterwards, aerosol growth slows down considerably, so that the peak aerosol mass of 110 $\mu\text{g}/\text{m}^3$ is reached only after 5 hours. The slow increase in aerosol mass in the beginning of the experiment is likely an important feature of the experimental data for determination of
295 mass transfer and chemical reaction rates.

The produced aerosol mass corresponds to a SOA yield of 130 % (Table 2) and is observed to be constant in the chamber for several hours at 5 °C. Note that this observation is different from previous experiments conducted at 25 °C and 40 °C (Boyd et al., 2017), where peak aerosol mass was achieved swiftly and SOA yields at aerosol mass loadings similar to this study were

Table 1. Fit parameters of the kinetic model. Error estimates for the volatility distribution (parameters f_{apin} and f_{lim}) can be found in Fig. S4 in the Supplement, error estimates for all other parameters are ranges in which a parameter can be varied until the model-experiment correlation decreases by 10 %. For a full list of kinetic parameters, see Table S1.

Parameter	Value of best fit	Description
$f_{\text{apin,org,b1}} - f_{\text{apin,org,b6}}$	see Fig. S4	Volatility distribution of non-nitrated α -pinene oxidation products
$f_{\text{apin,nitr,b1}} - f_{\text{apin,nitr,b6}}$	see Fig. S4	Volatility distribution of nitrated α -pinene oxidation products
$f_{\text{lim,org,b1}} - f_{\text{lim,org,b6}}$	see Fig. S4	Volatility distribution of non-nitrated limonene oxidation products
$f_{\text{lim,nitr,b1}} - f_{\text{lim,nitr,b6}}$	see Fig. S4	Volatility distribution of nitrated limonene oxidation products
$l_{\text{w,i}}$	$1.20 (0.97 - 1.51) \times 10^{-4}$	Transport rate in Teflon wall / irreversible loss rate (s^{-1})
$\Delta H_{\text{vap,apin}}$	81.3 (66.2 - 96.5)	Effective enthalpy of vaporization of α -pinene SOA products (kJ/mol)
$\Delta H_{\text{vap,lim}}$	164 (153 - 168)	Effective enthalpy of vaporization of limonene SOA products (kJ/mol)
C_{IM1}^*	$5.5 (0.89 - \infty) \times 10^5$	Saturation mass concentration, non-nitrated limonene SOA intermediate at 298 K ($\mu\text{g}/\text{m}^3$)
C_{IM2}^*	$7.43 (5.49 - 10.4) \times 10^3$	Saturation mass concentration, nitrated limonene SOA intermediate at 298 K ($\mu\text{g}/\text{m}^3$)
c_1	$1.96 (1.67 - 2.24) \times 10^{-2}$	Branching ratio, gas-phase dimer yield from $\text{RO}_2 + \text{RO}_2$
c_2	0.414 (0.381 - 0.451)	Branching ratio, RO yield from $\text{RO}_2 + \text{RO}_2$
$c_{3,\text{apin}}$	$5.93 (5.24 - 6.56) \times 10^{-2}$	Branching ratio, product yield from RO, α -pinene
$c_{3,\text{lim}}$	0.337 (0.236 - 0.478)	Branching ratio, product yield from RO, limonene
$c_{4,\text{apin}}$	0 (0 - 0.091)	Product ratio of non-nitrated to nitrated species from RO, α -pinene
$c_{4,\text{lim}}$	0.523 (0.303 - 0.730)	Product ratio of non -nitrated to nitrated species from RO, limonene
$k_{\text{form,apin}}$	0.124 (0 - 0.410)	Oligomerization rate coefficient, α -pinene (h^{-1})
$k_{\text{form,lim}}$	17.2 (15.5 - 18.9)	Oligomerization rate coefficient, limonene (h^{-1})
$k_{\text{decom,apin}}$	19.0 (7.45 - ∞)	Oligomer decomposition rate coefficient, α -pinene (h^{-1})
$k_{\text{decom,lim}}$	$9.00 (7.92 - 9.98) \times 10^{-2}$	Oligomer decomposition rate coefficient, limonene (h^{-1})
$E_{\text{A,decom,apin}}$	795 (0 - 1077)	Activation energy of oligomer decomposition, α -pinene (kJ/mol)
$E_{\text{A,decom,lim}}$	142 (112 - 180)	Activation energy of oligomer decomposition, limonene (kJ/mol)

determined to be 174 % and 94 %, respectively. While the lower SOA yield at 40 °C compared to 25 °C can be explained with equilibrium partitioning theory, the slightly lower mass yield observed at 5 °C in this study cannot.

After 7 hours of total experiment time, the temperature set point of the chamber enclosure is increased to 25 °C. The new temperature plateau is reached inside the Teflon chamber 90 minutes later (grey dashed line, right axis). The temperature change causes a slight reduction in aerosol mass from 110 to about 104 $\mu\text{g}/\text{m}^3$. At the new temperature set point, aerosol mass is not constant, but rather decays at a constant rate. After about 19 hours, the temperature set point is increased to 42 °C, which

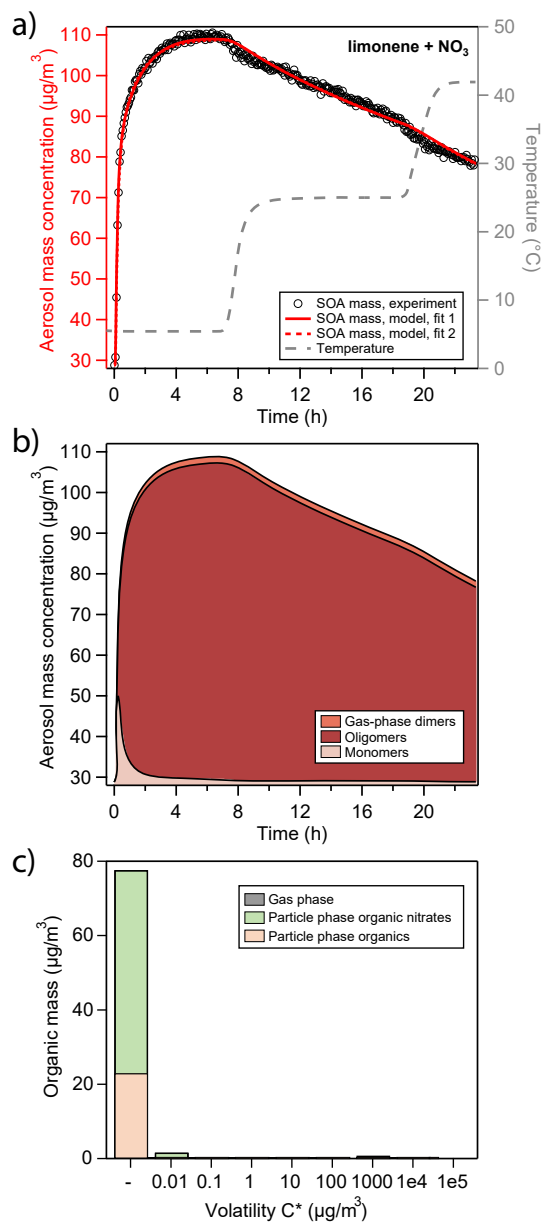


Figure 2. (a) Comparison of experimental and modelling results for oxidation of limonene with NO_3 . Open black markers are experimental aerosol mass obtained using an SMPS. The red solid line represents the best fit model result, the red dotted line an alternative model fit and the grey dashed line corresponds to the experimental temperature profile. (b) Analysis of the oligomerization state of particle-phase products in the model according to fit 1. (c) Analysis of the occupation of volatility bins of all products according to fit 1 and at peak SOA mass. Shadings in the bar plot denote where molecules of a certain volatility bin reside: gas phase (grey) or particle phase (colored). Products in the particle phase are further distinguished as organic nitrates (green) and non-nitrated organics (orange).

Table 2. Experimental conditions for environmental chamber experiments presented in this study alongside aerosol masses and SOA yields at 5 °C.

Exp	VOC 1 (ppb)	VOC 2 (ppb)	Experiment variant	Seed mass [†] (μg/m ³)	Peak total aerosol mass [†] (μg/m ³)	Peak SOA mass [†] (μg/m ³)	SOA yield (%)
LIM	limonene (10.5 ± 1.1)		pure limonene	28.8 ± 1.4	110 ± 5	81.3 ± 5.7	130 ± 16
APN	α-pinene (47.5 ± 4.8)		pure α-pinene	37.3 ± 1.9	109 ± 5	71.4 ± 5.7	25.2 ± 3.2
SEQ	α-pinene (24 ± 2.4)	limonene (5 ± 0.5)	sequential	33.4 ± 1.7	100 ± 5	66.7 ± 5.3	38.5 ± 4.9
MIX	α-pinene (22.5 ± 2.3)	limonene (5 ± 0.5)	simultaneous	40.9 ± 2.0	93.8 ± 4.7	52.9 ± 5.1	32.2 ± 4.5

†: Aerosol masses are calculated from aerosol volume concentrations using a density of (NH₄)₂SO₄ seed particles of 1.75 g/cm³, the organic phase of 1.64 g/cm³ for limonene SOA (Boyd et al., 2017), 1.46 g/cm³ for α-pinene SOA (Nah et al., 2016b), and 1.55 g/cm³ for the mixtures. SOA mass is calculated as the difference between peak total aerosol mass and pre-growth seed mass. All the reported masses are wall-loss corrected.

305 again causes an immediate slight reduction in aerosol mass from 90 to about 83 μg/m³. At the new temperature plateau of 42 °C, aerosol mass once again decays at a constant rate that is comparable to the one previously observed.

3.1.2 Kinetic modelling results (LIM)

In the following, kinetic modelling results are discussed in terms of a best fit (fit 1) that is obtained using the Monte Carlo Genetic Algorithm (MCGA). An alternative fit (fit 2) was obtained, but is indistinguishable from fit 1 for the LIM experiment.

310 The uniqueness of these fits and potential pitfalls of the optimization process are discussed in Sects. 3.5 and 4.

Under the conditions employed in this study, limonene precursor oxidation is dominated by NO₃ oxidation. RO₂ fate is dominated by reaction with NO₃ and RO₂ as very little NO and HO₂ are present in the chamber. The kinetic model (red solid and dotted line in Fig. 2a) is able to reproduce the observed aerosol formation and evaporation behavior. In the model run at hand, the initial quick increase in aerosol mass is due to condensation of dimers formed in the gas phase through the RO₂ + RO₂ channel (from now on referred to as “gas-phase dimers”), making up about 50 % of condensing material in the initial seconds. Subsequent growth is due to condensation of monomeric oxidation products (from now on referred to as “monomers”) of sufficiently low volatility (Fig. 2b). When half of the aerosol mass at peak growth is reached, the particle phase is to a large extent comprised of monomeric compounds, about 40 % of which still contain a C-C double bond (Fig. S5). These mono-unsaturated oxidation products either partition back into the gas phase where they can be oxidized further, or co-oligomerize in the particle phase with other oxidation products.

315
320

The vapor pressure of the non-nitrated and nitrated mono-unsaturated oxidation products were fitted during the MCGA optimization and determined to have saturation mass concentrations C^* of 5.5×10^5 and 7.43×10^3 μg/m³ at 298 K, respectively.

This means that the non-nitrated intermediate is fully volatile and the non-nitrated intermediate partitions to some extent into the particle phase. At peak SOA mass, 33 % of oxidation products still contain a double bond in this model run, all of which are nitrated and present as oligomers. Note that this is possible because we do not consider the oxidation of unsaturated compounds in the particle phase.

The volatility distribution key determined by global optimization can be found in Fig. S4. A large fraction of limonene oxidation products in this model run occupies the 6th and highest volatility bin ($C^* = 1 \times 10^5 \mu\text{g}/\text{m}^3$ at 298 K), which is mostly present in the gas phase under these reaction conditions. Fig. 2c shows the resulting volatility distribution of organics in the particle phase according to the model at peak growth, which lacks organic material from the highest volatility bin. In the model, the slow increase in aerosol mass from about $80 \mu\text{g}/\text{m}^3$ to $110 \mu\text{g}/\text{m}^3$ is due to oligomerization of monomers forming higher molecular weight structures through accretion reactions in the particle phase (from now on referred to as “oligomers”). According to the model fit, oligomerization occurs at a rate of $k_{\text{form,lim}} = 17.2 \text{ h}^{-1}$. Barsanti et al. (2017) compiled accretion rate coefficients with relevance to SOA formation and report rate coefficients for hemiacetal formation under neutral conditions in methanol of $0.1 \text{ M}^{-1}\text{s}^{-1}$ and peroxyhemiacetal formation of $0.5\text{--}70 \text{ M}^{-1}\text{s}^{-1}$. Assuming that every limonene oxidation product has two reactive sites to undergo oligomer formation, $k_{\text{form,lim}}$ can be translated into a second-order reaction rate coefficient of $1.4 \text{ M}^{-1}\text{s}^{-1}$ and thus lies in close proximity to literature values.

Oligomerization slowly removes semi-volatile species in the particle phase from the partitioning equilibrium, which in turn causes a flux of semi-volatile molecules from the gas phase into the particle phase. The highest volatility components partition into the particle oligomer phase slowest, causing the slow increase of limonene SOA mass over 5 hours. Quantum chemical and mechanistic studies have previously predicted such pronounced differences between the volatility of typical oxidation products of monoterpenes and their oligomers of several orders of magnitude (DePalma et al., 2013; Barsanti et al., 2017).

At peak SOA mass, the model predicts most of the organic material in the particle phase to exist in an oligomeric state (Fig. 2b), which explains the lack of initial evaporation caused by an increase in chamber temperature. A model fit to the LIM experimental data was attempted without inclusion of particle-phase oligomerization reactions. The model output of this simulation run shows an overall low correlation to the experimental data as it cannot explain the long time to reach peak SOA mass and the slow mass decrease at $42 \text{ }^\circ\text{C}$ (Fig. S6).

The slow decay of aerosol mass between 6 and 24 hours of the experiment is attributed in the model to a slow unimolecular decay of oligomeric material with a rate of 0.09 h^{-1} and subsequent evaporation of monomers at elevated temperatures, followed by deposition and irreversible loss of vapors on the chamber walls. The decomposition rate suggested by the model agrees well with the rate of $0.06\text{--}0.2 \text{ h}^{-1}$ reported by (D’Ambro et al., 2018) for SOA formed from ozonolysis of α -pinene. Following Le Chatelier’s principle, removal of monomers from the equilibrium causes a constant flux of organic matter from oligomeric to monomeric state. Since the volatility of the monomeric subunit is retained in the model, this process is faster for monomers that have higher volatilities because they partition into the gas phase more quickly and readily, causing an enrichment of low-volatility monomeric subunits in the particle phase. The (meta-)stability of organic material in the particle phase can hence be attributed not only to the stability of the oligomer bond, but also the volatility of the monomeric building blocks at that temperature.

Monomers are removed from the system by deposition onto and diffusion into the chamber walls, which is the main driver of loss of organic mass. The irreversible loss rate of wall-adsorbed molecules into the chamber wall is determined to be $l_{w,i} = 1.2 \times 10^{-4} \text{ s}^{-1}$, which is within the range of values reported as re-evaluation from literature data in Fig. 5 of Huang et al. (2018). Fig. S7 shows the distribution of organic molecules between wall, particle and gas phase in the model for all experiments conducted in this study. The dependence of model output on $l_{w,i}$ is explored in Fig. S8, indicating that the model output simulating the LIM experiment is more sensitive to changes in $l_{w,i}$ than the simulation of the APN experiment described below, which can be attributed to the slow uptake and oligomerization process of semi-volatile molecules that stands in competition with irreversible wall loss.

The global optimization returned a value of 164 kJ/mol for the effective enthalpy of vaporization ΔH_{vap} of limonene oxidation products. This number stands in contrast to values used for monoterpenes in SOA models such as ECHAM-HAM (59 kJ/mol; Saathoff et al., 2009), GEOS-Chem (42 kJ/mol; Chung and Seinfeld, 2002) or GISS-modelE (72.9 kJ/mol; Tsigaridis et al., 2006), but agrees with the value of about 160 kJ/mol obtained in Boyd et al. (2017) at a similar mass loading. Boyd et al. compared SOA yields at two different temperatures for a range of initial precursor concentrations and determined ΔH_{vap} based on the Claudius-Clapeyron equation. A sensitivity study on the effect of ΔH_{vap} on model output is shown in Fig. S9.

The results obtained in this study can be compared to and used to interpret results in a previous study by Boyd et al. (2017). This study observes a lower SOA yield at 5 °C (130 %) compared to the previous experiments performed at 25 °C (174 %). This finding cannot be explained by gas-particle partitioning alone, as lower temperatures should give rise to higher SOA yields. A probable cause could be the temperature dependence of the gas phase oxidation chemistry, however, test calculations using the temperature-dependent rate coefficients reported in the MCM mechanism showed hardly any effect of temperature on SOA yield. Thus, another promising explanation is the temperature dependence of the oligomerization rate coefficient. As the model calculations highlight, condensation of vapors onto the suspended particles stands in competition with loss to the chamber walls, which should not be strongly temperature-dependent. When oligomerization occurs more slowly, oxidation products from higher volatility bins are increasingly lost to the walls before they can be incorporated into the particle oligomer phase. This is confirmed by a sensitivity study that shows a strong influence of oligomer formation rate $k_{\text{form,lim}}$ on model output (Fig. S10). In addition to temperature dependence of the rate coefficient itself, oligomerization turnover might be effectively depressed by a semi-solid phase state at 5 °C as discussed in Sect. 3.5.3.

Another observation in Boyd et al. (2017) was a lower SOA mass when directly forming limonene SOA at 40 °C compared to first forming limonene SOA at 25 °C and then heating to 40 °C. This observation could also be explained by the successive condensation and oligomerization of semi-volatile vapors suggested by the model in this study. The fraction of chemical species from the higher volatility bins that partitions into the particle phase is much smaller at 40 °C compared to 25 °C. This may prevent the additional slow mass accumulation through oligomerization of semi-volatile oxidation products at 40 °C and result in a lower SOA yield.

3.2 Pure α -pinene oxidation (APN)

3.2.1 Experimental observations (APN)

Fig. 3a shows the aerosol mass during the corresponding experiment of α -pinene oxidation with NO_3 , here referred to as “APN” experiment. Similar to the LIM experiment described above, oxidation at 5 °C initially causes a fast increase in aerosol mass (black open markers), however, peak aerosol mass is **already reached** after 3 hours of oxidation at 109 $\mu\text{g}/\text{m}^3$ **and a corresponding SOA yield of 25.2 % (Table 2). At a comparable organic mass, this yield is significantly lower than observed in the limonene oxidation experiment. Note that, in order to achieve similar aerosol mass loadings among all experiments in this study, a larger amount of precursor is added in the α -pinene oxidation experiment.**

The SOA yield in this study appears to be larger than previously reported for the oxidation of α -pinene with NO_3 : Hallquist et al. (1999) measured a 7 % yield (corresponding to 52.9 $\mu\text{g}/\text{m}^3$ organic aerosol) at 15 °C. Nah et al. (2016b) measured a yield of 3.6 % (corresponding to 2.4 $\mu\text{g}/\text{m}^3$ organic aerosol) at room temperature. Fry et al. (2014) reported no significant aerosol growth at room temperature. This is indicative of the low temperature employed in the experiments having a significant impact on SOA yield.

After about 4 hours of total experiment time, the temperature set point of the chamber enclosure is increased to 25 °C, leading to a sharp and significant evaporation of organic material from aerosol particles. When the new temperature plateau is reached after 7 hours, aerosol mass has decreased to 80 $\mu\text{g}/\text{m}^3$. Since evaporation has hardly slowed down by that time, heating to the new temperature set point of 42 °C is initiated after 8 hours of experiment time (i.e., without long waiting time at the 25 °C temperature plateau) to avoid losing too much volatile aerosol mass from evaporation. After a chamber temperature of 42 °C is reached after 10 hours, evaporation slows down considerably and continues at a slow rate until the end of the experiment, where a minimum aerosol mass of 57 $\mu\text{g}/\text{m}^3$ is observed. With a seed mass of 37.3 $\mu\text{g}/\text{m}^3$, this corresponds to a retained organic aerosol mass of about 20 $\mu\text{g}/\text{m}^3$ (cf. Table 2).

3.2.2 Kinetic modelling results (APN)

The kinetic model (blue solid line in Fig. 3a) shows a reasonable correlation to the experimental data. The detailed model analysis in Fig. 3b reveals that at peak SOA mass, the aerosol is composed of about 73 % of monomers, 5 % oligomers and 22 % gas-phase dimers (Fig. 3b). These monomers mostly occupy the $C^* = 1 - 100 \mu\text{g}/\text{m}^3$ volatility bins (Fig. 3c). Note that in Fig. 3c, a large fraction of α -pinene oxidation products occupies the $C^* = 1 \times 10^5 \mu\text{g}/\text{m}^3$ volatility bin, which explains the overall low SOA yield.

Upon increase in chamber temperature, evaporation of monomers in volatility bins $C^* = 10 - 100 \mu\text{g}/\text{m}^3$ and decomposition of oligomers lead to a decrease of the monomer and oligomer mass, respectively. As a result, the gas-phase dimers represent a greater fraction of the total condensed mass and their mass fraction increases from 22 % to 74 %. Hence, the slowing of evaporation of organic material toward the end of the experiment can be attributed to the fact that the remaining organic aerosol is only comprised of gas-phase dimers ($C^* = 0.01 \mu\text{g}/\text{m}^3$), low-volatile monomers ($C^* = 0.01 - 1 \mu\text{g}/\text{m}^3$ volatility bins) and oligomers composed of low-volatile monomer building blocks.

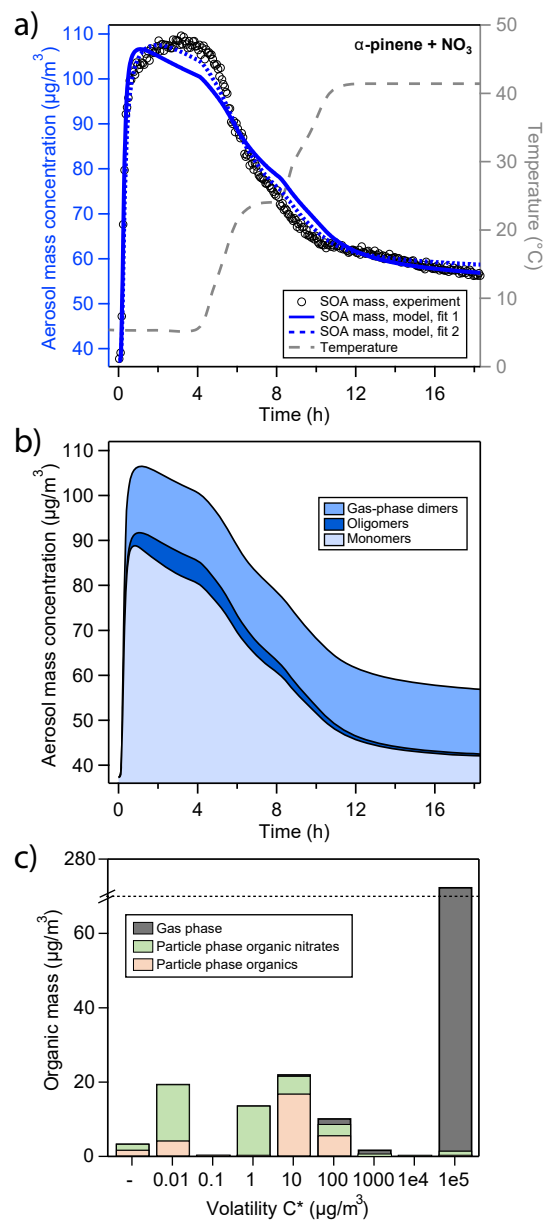


Figure 3. (a) Comparison of experimental and modelling results of aerosol mass for oxidation of α -pinene with NO_3 . Open black markers are experimental aerosol masses obtained using an SMPS. The blue solid line represents the best fit model result, the blue dotted line an alternative model fit and the grey dashed line corresponds to the experimental temperature profile. (b) Analysis of the oligomerization state of particle-phase products in the model according to fit 1. (c) Analysis of the occupation of volatility bins of all products according to fit 1 and during peak SOA mass. Shadings in the bar plot denote where molecules of a certain volatility bin reside: gas phase (grey) or particle phase (colored). Products in the particle phase are further distinguished as organic nitrates (green) and non-nitrated organics (orange).

Compared to the LIM experiment, peak aerosol mass is reached more quickly in the APN experiment, which is even exaggerated in the model solution. In the model, the oligomer formation rate is low at 0.124 h^{-1} , which is two orders of magnitude slower than determined for the LIM experiment. On the other hand, the oligomer decomposition rate is determined to be 19.0 h^{-1} , which is two orders of magnitude quicker than that determined for the LIM experiment and the rates reported by D'Ambro et al. (2018) for SOA from α -pinene ozonolysis. This leads to an overall lower, more labile oligomer content for the APN experiment **according to the model**. The higher gas-phase dimer concentration can be explained by the higher initial precursor concentration used in the APN experiment that leads to a higher momentary RO_2 concentration (cf. Fig. S11) and hence a more pronounced $\text{RO}_2 + \text{RO}_2$ gas-phase chemistry compared to the LIM experiment. **The branching coefficient c_1 for dimer formation (cf. Fig. S3) is not included in the original MCM mechanism, but was determined here from the inverse modelling to be 1.96×10^{-2} .**

The effective enthalpy of vaporization ΔH_{vap} of α -pinene oxidation products is determined to 81.3 kJ/mol , which is only slightly larger than values used in the SOA models ECHAM-HAM (59 kJ/mol ; Saathoff et al., 2009), GEOS-Chem (42 kJ/mol ; Chung and Seinfeld, 2002) or GISS-modelE (72.9 kJ/mol ; Tsigaridis et al., 2006).

Fig. 3a also shows an alternative fit to the experimental data (fit 2). While this fit scored overall lower in our metric for model-experiment correlation, mostly due to misrepresentation of particulate organic nitrate content (pON/OA, cf. Sect. 3.4), it leads to a better representation of SOA mass for the APN experiment. In fit 2, oligomer fraction is overall higher, leading to a slower increase and slower decline of SOA mass, which is more in line with experimental data. This is achieved by a much faster oligomerization rate of 9.0 h^{-1} and a slower oligomer decomposition rate of 5.8 h^{-1} (Table S2). The oligomerization state of SOA according to fit 2 in analogy to Fig. 3b is shown in Fig. S12, the fit parameters for both, fits 1 and 2, are compared in Table S2. A discussion of the inability of the model to fit both SOA mass and pON/OA for α -pinene at the same time can be found in Sect. 3.5.3.

3.3 Simultaneous and sequential oxidation experiments (MIX and SEQ)

In addition to oxidation experiments with single precursors, experiments are performed where α -pinene and limonene are oxidized simultaneously (MIX) or in sequence (SEQ) to investigate whether their co-existence affects growth or evaporation of SOA. In Figs. 4a (MIX) and 4b (SEQ), aerosol mass is displayed for these two scenarios alongside kinetic modelling results. The experiments are set up in a way that the produced aerosol mass is comparable in magnitude to the pure precursor experiments and both precursors contribute to the produced mass in equal parts. Table 2 lists the experimental SOA yields along with injected precursor amounts.

3.3.1 Experimental observations (MIX and SEQ)

In the MIX experiment (Fig. 4a), most of the initial increase in aerosol mass (black open markers) is rapid and peak SOA mass is reached after about 3 hours, comparable to the pure α -pinene oxidation experiment. The evaporation pattern upon chamber heating shows a less pronounced decrease in particle mass compared to the APN experiment, but is more pronounced than

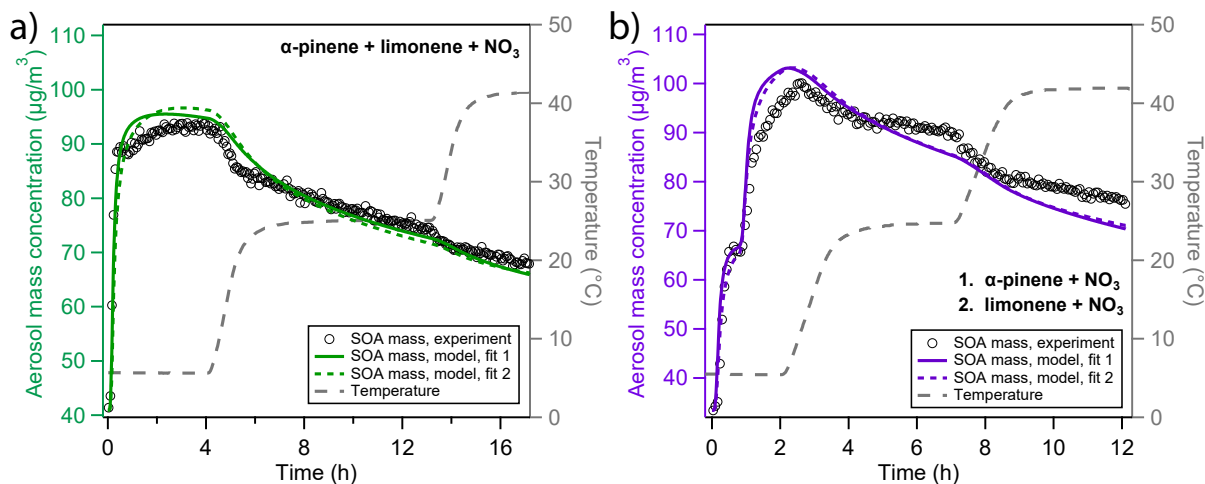


Figure 4. Overview of experimental and modelling results of aerosol mass for experiments with mixed monoterpene precursors. The experiments in the two panels differ in the way the precursors were added: (a) simultaneous oxidation of a mixture of α -pinene and limonene, (b) sequential oxidation of firstly α -pinene and secondly limonene with NO_3 . Open black markers are experimental aerosol mass obtained using an SMPS. The colored solid and dotted lines represent model results from two different fits to the experimental data. The grey dashed line indicates the experimental temperature profile.

observed in the LIM experiment. Overall, the mass loss during the 5 °C to 25 °C evaporation step is more pronounced than mass loss during the 25 °C to 42 °C step.

In the SEQ experiment (Fig. 4b), initial growth of α -pinene SOA onto the inorganic seed particles is rapid. After subsequent injection of limonene precursor, the second increase in aerosol mass is more gradual, as would be expected from the pure LIM experiment. This might be due to slow formation of oligomers, but also simply because the lower amount of limonene precursor and proportionately lower injected NO_3 leads to a longer reaction time. However, the modelled reaction times for α -pinene and limonene to reach 5 % of their initial concentration after precursor injection were both about 15 minutes (cf. Fig. S11), which is a short time frame in comparison to the slow increase of limonene mass. The evaporation pattern in the SEQ experiment is less pronounced than the one in the MIX experiment during the 5 °C to 25 °C temperature increase and equally marginal from 25 °C to 42 °C.

3.3.2 Kinetic modelling results (MIX and SEQ)

The model result of the best fit modelling scenario (fit 1, solid green and purple lines) shows fair correlation to the experimental data in the MIX experiment (Fig. 4a), but lacks in correlation in the SEQ experiment (Fig. 4b). The alternative modelling scenario (fit 2, dotted green and purple lines) shows very similar behavior. Strikingly, the mass at peak aerosol growth is overestimated by the model in both scenarios. Furthermore, initial evaporation is overestimated such that aerosol mass in the middle and late stages of the experiments agrees between model and experiment for the MIX experiment. Towards the end of

the experiment, evaporation is further overestimated in the SEQ experiment, such that predicted aerosol mass becomes lower than the experimentally observed mass.

We note that, while peak mass does not coincide between model and experiment for the MIX and SEQ experiment, it is possible to obtain model fits in which this is the case. It is however not possible to match both, the peak mass and the experimentally-observed evaporation pattern. Slight overestimation of peak mass in the fits at hand can hence be seen as a consequence of the optimization algorithm trying to minimize the least squares error when in reality the evaporation pattern could not be reproduced.

Fig. S13 shows the time evolution of α -pinene- and limonene-derived oxidation products over time in the MIX and SEQ experiments. More α -pinene than limonene oxidation products evaporate from the particles in these model simulations, as would be expected from the pure precursor experiments. However, the fact that model-experiment correlation in the MIX and SEQ experiments is worse than in the APN and LIM experiments indicates non-linear behavior of the mixed precursor experiments. Because evaporation is overestimated by the model, especially in the SEQ experiment, effects not treated in the current model must lead to a slowing of evaporation speed in the mixed precursor experiments.

These results are similar to the findings of Boyd et al. (2017), who showed less evaporation of limonene SOA and more evaporation of β -pinene SOA in a SEQ-type experiment (β -pinene SOA condensing on preformed limonene SOA) compared to their MIX-type experiment. The study postulated a core-shell morphology of a limonene SOA core and a β -pinene SOA shell that is sustained due to incomplete mixing, though oligomerization between limonene and β -pinene oxidation products could also play a role. Here, we show in a proof of concept that oligomerization mechanics alone cannot fully explain the evaporation of monoterpene SOA mixtures. In Sect 3.5, we will take a closer look at possible explanations.

3.4 Organic nitrate fractions

In this study, the organic nitrate fraction (pON/OA) is presented as ratio of the total mass concentration of particulate ON (which includes the organic part and nitrate part of the ON compounds) to the total mass concentration of organic aerosol (which includes both ON and non-nitrated organics) (Takeuchi and Ng, 2019). It can be inferred from AMS data using Eq. 10. In this formula, it is assumed that all organic aerosol mass is found in the organic and nitrate signal of the AMS (AMS_{ORG} and AMS_{NO_3}) and all AMS nitrate is ON. When MW_{pON} is the average molar mass of the ON (i.e., 250 g/mol in this study) and MW_{NO_3} the molar mass of the nitrate group (i.e., 62 g/mol), the pON mass can be determined by scaling the AMS signal with the ratio of these molar masses.

$$\frac{\text{pON}}{\text{OA}} = \frac{AMS_{\text{NO}_3} \cdot \frac{MW_{\text{pON}}}{MW_{\text{NO}_3}}}{AMS_{\text{NO}_3} + AMS_{\text{ORG}}} \approx \frac{4.03}{1 + \frac{AMS_{\text{ORG}}}{AMS_{\text{NO}_3}}} \quad (10)$$

Fig. 5 depicts measured and modelled values of pON/OA for all four experiments. Panel a shows that in the LIM experiment, pON/OA is high, with a mass ratio of about 0.8 in the particle phase, and only slightly increases over time, which is reproduced in the model. An alternative representation, showing the contribution of dinitrated, mononitrated and non-nitrated organics to SOA mass, is shown in Fig. S14 in the Supplement and reveals that despite the high pON/OA, a significant fraction of products remains non-nitrated and the high pON/OA is caused by the presence of dinitrated oxidation products. Note that the average

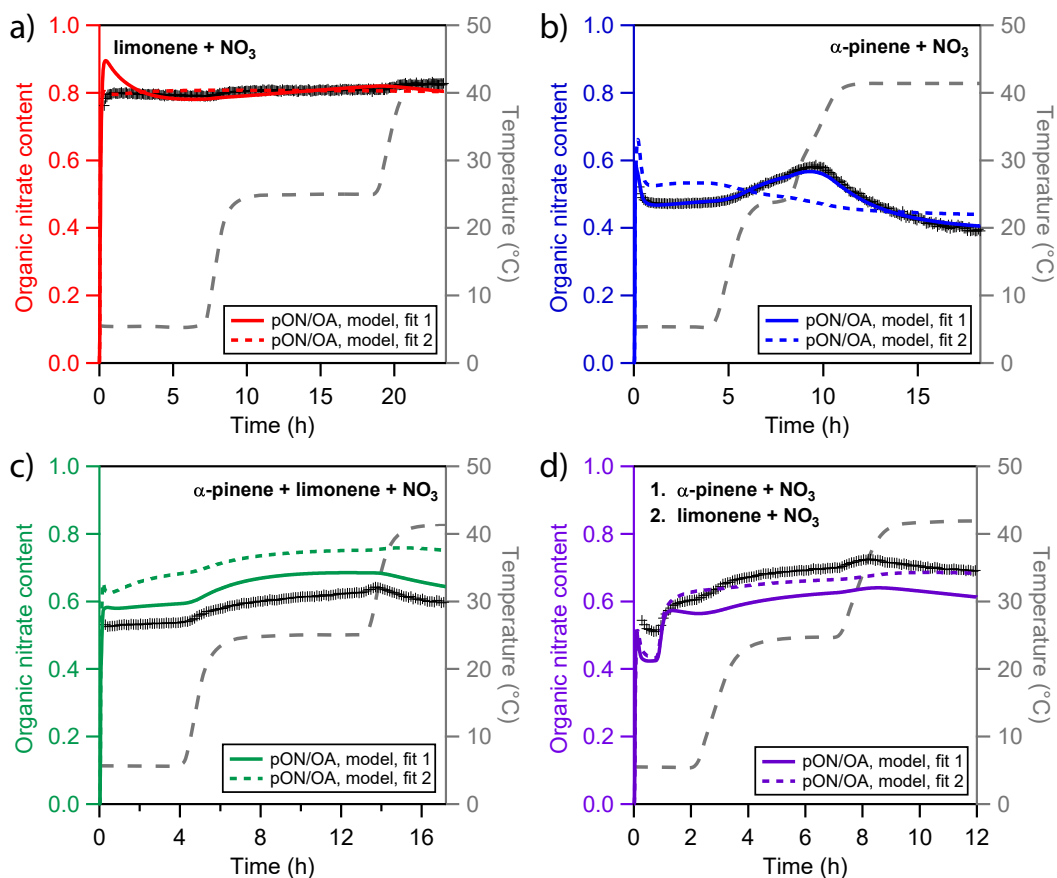


Figure 5. Experimental and modelling results of particulate organic nitrate content (pON/OA) for four different types of chamber-generated SOA. (a) only limonene, (b) only α -pinene, (c) a mixture of α -pinene and limonene and (d) sequential oxidation of firstly α -pinene and secondly limonene. Cross markers are experimental nitration degrees inferred using a High Resolution Time-of-Flight Aerosol Mass Spectrometer (HR-ToF-AMS). The colored solid and dotted lines represent results of the kinetic model. The grey dashed line indicates the experimental temperature profile.

505 molar mass of ON might change during the experiment, e.g., by evaporation of lower molecular weight components, which is not considered in our calculation. In the model, the slow evaporation of limonene SOA is caused by oligomer decomposition followed by evaporation of volatile monomers. The fact that pON/OA is rather constant over time thus gives no evidence that decomposition rates of oligomers consisting of nitrated or non-nitrated monomeric building blocks might differ and we use the same oligomer decomposition rate irrespective of nitration state of the product bin. Note that in the absence of oligomerization,

510 a constant pON/OA could only be obtained if nitrated and non-nitrated organics were evenly distributed across the evaporating volatility bins. Panel b shows pON/OA in the APN experiment. The initial nitrate content is lower than in the LIM experiment with a value of about 0.45. During the first temperature increase in the APN experiment, ON content increases with the reduc-

tion in organic mass, indicating predominant evaporation of non-nitrated oxidation products. During the second evaporation step, ON content decreases, indicating predominant evaporation of nitrated oxidation product. The best fit model run (solid blue line) captures the ON content very well. As Fig. 3b highlights, the model suggests the higher-volatility monomers to be non-nitrated and the lower-volatility monomers to be nitrated, which causes the distinct trend of pON/OA. The alternative model run (dotted blue line), however, fails to capture the ON time dependence. This is due to the high oligomer content of fit 2 and due to the model not distinguishing between nitrated oligomer and non-nitrated oligomer decomposition rates. Hence, while the oligomer-heavy fit 2 shows a better correlation to α -pinene SOA mass, it fails at describing pON/OA.

The measured and simulated ON contents for the experiments with multiple precursors are shown in panels c and d of Fig. 5 for the MIX and SEQ experiment, respectively. While both experiments use approximately the same concentrations of α -pinene and limonene, the measured pON/OA are slightly different. Simultaneous oxidation (MIX) leads to an initial pON/OA of 0.53, which is surprisingly low and closer to the value measured for pure α -pinene SOA. Sequential oxidation (SEQ) leads to an initial pON/OA of 0.52 after α -pinene oxidation, and increases to 0.6 after oxidation of limonene has concluded. This value in the SEQ experiment is closer to the expected value when assuming linear additivity of ON content. The unexpectedly low ON content in the MIX experiment points either towards non-linear effects in chemistry that are not captured by the model or towards uncertainties in the pON/OA measurements. For the latter, there are two major sources of uncertainty. First, a default value of relative ionization efficiency (RIE) of 1.1 is used for AMS nitrate in this study (Canagaratna et al., 2007). This value is typically associated with inorganic nitrate as the RIE of nitrate derived from pON has not yet been experimentally measured to the knowledge of the authors. It is thus not clear how this value depends on chemical composition or if exposure to higher temperature may lead to variation of RIE over the course of an experiment. Second, a constant molecular weight of pON (250 g/mol) is assumed for calculation of pON/OA. However, it is possible that changes in chemical composition result in changes of the average molecular weight during an experiment. However, qualitatively, the time and temperature dependence of the ON fraction is overall captured well by the model for the mixed precursor experiments. In both cases, predominant evaporation of α -pinene oxidation products, which are the more-volatile and less-nitrated components of the mixture, leads to an increase of pON/OA until the highest temperature.

The model parameters that mainly determine pON/OA are the volatility distributions of the nitrated and non-nitrated oxidation products, but also the branching coefficients of the gas phase chemical mechanism (cf. Fig. S3). The chemical mechanism presented in this study deviates from the MCM template in that it allows nitrated alkoxy radicals ($R^N O$) to stabilize without elimination of the nitrate function. This is realized in the model using a branching coefficient c_4 that determines the fraction of $R^N O$ that loses its nitrate group during the conversion to a stable oxidation product. c_4 is determined to be 0 for the α -pinene system and 0.52 for the limonene system, both indicating a significant retrieval of stable organic nitrates from nitrated alkoxy radicals. A small value of c_4 stands in contrast to the findings of Kurtén et al. (2017), who ascribed the low organic nitrate yield in the oxidation of α -pinene with NO_3 to a predominant stabilization of $R^N O$ to the volatile and non-nitrated pinonaldehyde. Note that these calculations were performed at 25 °C, while α -pinene oxidation occurred at 5 °C in our experiments and model. c_4 itself is unlikely to have a positive temperature dependence, as the reaction pathway with the lower activation barrier should be even more favored at lower temperature. However, it may be possible that the fraction of alkyl

radicals that undergo rearrangement (Vereecken et al., 2007) is enhanced at low temperature. The peroxy and alkoxy radicals resulting from such a rearrangement do not lose NO_2 upon stabilization. In addition, oxidation products with aldehyde moieties might be nitrated in a secondary reaction with NO_3 (Atkinson and Arey, 2003). This represents another channel of increasing pON/OA and is not considered in our model. Thus, the simple gas-phase chemistry branching coefficients c_2 - c_4 obtained through inverse modelling may be seen as effective parameters that represent gas-phase radical chemistry in the context of a certain experiment and volatility distribution, but their numerical values should not be evaluated in isolation.

A notable observation from modelling is that dimers from the gas-phase reaction of $\text{RO}_2 + \text{RO}_2$ are mainly nitrates because most RO_2 radicals originate from the reaction of alkene with NO_3 and are hence nitrated. This is especially significant for the α -pinene + NO_3 reaction system since the high momentary RO_2 radical concentrations in these experiments lead to a high estimated contribution of gas-phase dimers to aerosol mass of 22 % at peak SOA mass and 74 % after heating to 42 °C (cf. Fig. 3).

In summary, the experimental and modelling results in this study confirm previous studies and report a high efficiency of nitration in the reaction of monoterpenes with NO_3 , with a nitrated SOA fraction larger than 50 % under most experimental conditions studies (Ng et al., 2017, and references therein). Limonene SOA shows overall higher nitration degrees than α -pinene SOA, which can be understood by the higher number of double bonds of the VOC precursor compound itself and hence more possibilities to introduce a nitrate group during oxidation. The temporal evolution of limonene SOA pON/OA was constant, which can be explained with a particle phase mostly consisting of oligomers whose decomposition rates do not differ for nitrated and non-nitrated building blocks. The temporal evolution of α -pinene SOA pON/OA can only be retrieved if the particle phase is predominantly comprised of monomers: sequential evaporation of nitrated and non-nitrated monomers with different vapor pressure leads to modulation of pON/OA.

3.5 Deviation between model and experiment

From Sect. 3.3, we can conclude that while peak aerosol mass can be reconciled between the four simulated experiments with the kinetic model, the evaporation pattern in experiments MIX and SEQ cannot be brought fully into agreement with the pure precursor experiments LIM and APN. Hence, the kinetic model must lack a process that leads to resistance in evaporation in the mixed precursor scenarios compared to the pure precursor experiments. Possible mechanisms introducing such non-linearity include:

1. Non-linear gas-phase chemistry
2. Augmented particle-phase oligomerization chemistry
3. Mass transfer limitations

In general, none of these points can be fully excluded based on the results presented in this manuscript. However, in the following, we will go through the obtained evidence and evaluate these points to make an informed guess on how likely they are to affect aerosol formation and evaporation.

580 3.5.1 Gas-phase chemistry

Non-linear effects in gas-phase chemistry branching ratios could lead to a mixture of oxidation products that is more readily oxidized or dimerized and hence would show a reduced evaporation rate upon increase in chamber temperature. One possible mechanism for this is an increased yield of gas-phase dimers due to bimolecular reaction of two RO₂ radicals from different precursors, forming hetero-dimers of oxidation products. Formation of hetero-dimers is considered in the model, however, the
585 branching ratio is assumed to be similar for limonene- and α -pinene-derived molecules and hence self-reactions are of the same speed as cross-reactions. Berndt et al. (2018) showed that cross-reactions of two different α -pinene-derived RO₂ radicals can be faster than the respective self-reaction rates. If such an effect existed for heterodimers of α -pinene and limonene oxidation products, this would cause a higher dimer fraction in the product spectrum, which in turn would lead to reduced evaporation of SOA from precursor mixtures due to overall lower volatility. Since in precursor mixtures the number of RO₂ radicals is
590 diversified, more cross-reactions will occur naturally, which would lead to more gas-phase dimers and in turn explain the slower evaporation in the MIX experiment. The SEQ experiment, however, also shows slow evaporation compared to the pure precursor experiment. Since oxidation occurred separately and cross-reactions are not enhanced by diversification of RO₂ radicals, formation of hetero-dimers in the gas phase cannot be the cause for reduced product volatility in the SEQ experiment.

Of note, any explanation for a decreased volatility of oxidation products due to gas-phase chemistry would not only change
595 the evaporation behavior of the SOA mixture, but also likely alter the SOA yield. This is because a general reduction in volatility not only causes products to remain in the particle phase at elevated temperature, but also causes products to partition into the particle phase at low temperature in the first place. Elevated SOA yields are not observed and it is hence unlikely that altered gas-phase chemistry leads to the observed reduced evaporation rates of the SOA mixtures.

3.5.2 Oligomerization

600 Augmented oligomerization in the particle phase is a possible explanation of reduced evaporation rates in case mixtures of oxidation products from different precursors oligomerize more readily together than the pure components in isolation. Unlike the gas-phase chemistry scenarios described above, these effects could be observed in both, MIX and SEQ experiments, since particle-phase oligomerization may occur retroactively after the second oxidation step in the sequential oxidation experiment. Moreover, oligomerization of already low-volatile products would not alter SOA yields as strongly as gas-phase chemical
605 effects would, but could have a pronounced influence on evaporation rates.

In general, an augmentation effect leading to a higher oligomerization degree in mixtures could be achieved when the hetero-oligomers were formed more efficiently than a linear combination of formation rates of both homo-oligomers. A similar effect would be achieved when oxidation products of one of the two precursors were such efficient oligomer-formers that they would cause the oxidation products of the other precursors to oligomerize more readily and pull them into the oligomer
610 phase. Therefore, during development of the model, we tested an implementation of the oligomerization scheme where formation of hetero-oligomers occurs at a combined rate using their logarithmic mean value, but first-order decomposition rates remain unaffected by the precursor type. The model solution exhibited a large discrepancy in oligomerization rates of a few

orders of magnitudes, with limonene oxidation products oligomerizing quickly and readily and α -pinene oxidation products hardly oligomerizing in isolation. As a result, mixtures of oxidation products still oligomerized significantly, driven by the high individual oligomer formation rate of limonene oxidation products. Equilibrium oligomerization degree is governed by both
615 oligomer formation and decomposition rates, but is also naturally capped to a value of 100 %. Hence, in conclusion, mixing a strong oligomer former that reaches this cap in isolation with a weak oligomer former can lead to a higher combined oligomerization degree of the mixture. However, this pure theoretical result seems unphysical as it requires a very high oligomerization degree of pure limonene SOA and a very small degree of oligomerization in pure α -pinene SOA, which has not been observed
620 in experimental studies (Faxon et al., 2018; Takeuchi and Ng, 2019).

3.5.3 Mass transfer limitations

Increased mass transfer limitations caused by high viscosity can cause a reduction of volatilization. This is due to surface concentrations of the evaporating components being depleted when the mixing time scale in the particle is longer than the evaporation time scale. Mass transfer limitation is not treated in the model runs previously shown in this study. Instead, a
625 well-mixed bulk phase is assumed and any resistance in evaporation is explained with oligomerization reactions. The slow evaporation of limonene SOA is hence solely caused by significant oligomerization in the model runs previously presented, but could also be caused by mass transfer limitations induced by a high bulk-phase viscosity, especially if a high fraction of particle-phase oligomers would have formed that depresses mobility of molecules in the condensed phase (Baltensperger et al., 2005; D'Ambro et al., 2018). Hence, limonene SOA might exhibit a more viscous phase state than α -pinene SOA. The high
630 viscosity caused by limonene oxidation products might in turn affect evaporation in the mixed precursor experiments and cause the observed non-linear effects.

In a first approximation, viscosities of mixtures can be assumed to be a linear combination of the individual viscosities and follow a logarithmic mixing rule (Gervasi et al., 2019). This entails that the change in the rate of mass transport between pure compounds and their mixtures can reach orders of magnitudes. This would be in line with volatilization rates observed in
635 the mixed precursor experiments being more similar to the pure LIM experiment, which was observed in this and a previous study (Boyd et al., 2017). Notably, while evaporation steps immediately following a change in chamber temperature are overall similar between the MIX and SEQ experiments, the slope of the aerosol mass versus time curve is steeper in the MIX experiments. This might suggest that in the SEQ experiment, limonene SOA might be covering the preformed α -pinene oxidation products in a core-shell morphology and thus hampering their volatilization.

To test the effect of impeded bulk diffusivity on the evaporation of SOA, we perform a sensitivity study in which we
640 increase viscosity in the model to evaluate whether the evaporation rates in the MIX and SEQ experiments can be brought into agreement with observations. We use the best case fitting scenario shown in Fig. 2 and raise the viscosity in the simulation to 1×10^7 Pas (Fig. 6). This viscosity is in the typical range for SOA under dry conditions and fall into the semi-solid phase state region (Koop et al., 2011; Shiraiwa et al., 2011; Abramson et al., 2013; Zhang et al., 2015; Grayson et al., 2016; Gervasi
645 et al., 2019). Using the Stokes-Einstein relation (Einstein, 1905) and an effective molecular radius of 2 nm, this viscosity corresponds to a bulk diffusion coefficient of 1×10^{-16} cm²/s at 298 K. The effective radius is approximated from geometric

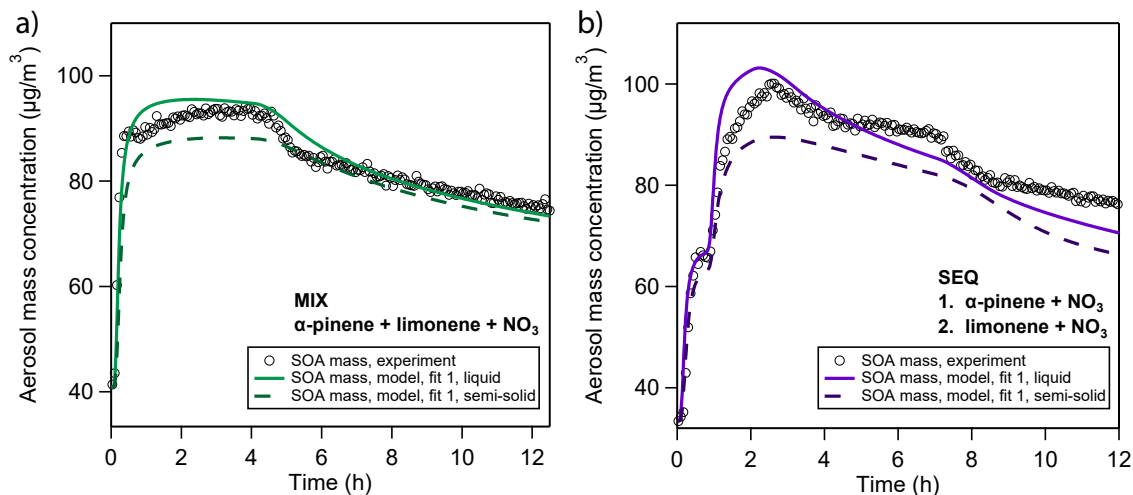


Figure 6. Sensitivity study on the influence of viscosity on model simulation results based on the best case fitting scenario in the (a) MIX and (b) SEQ experiments. Model simulations were performed for the default well-mixed case (solid lines) and at a diffusivity coefficient of $1 \times 10^{-16} \text{ cm}^2/\text{s}$, which corresponds to a bulk viscosity of $1 \times 10^7 \text{ Pa}\cdot\text{s}$ according to the Stokes-Einstein relation and falls within the semi-solid phase state range.

considerations assuming spherical molecular shape, a molar mass of $250 \text{ g}/\text{mol}$ and density of $1.55 \text{ g}/\text{cm}^3$. The temperature dependence of this diffusion coefficient is approximated with a constant activation enthalpy of diffusion $\Delta H_{\text{dif}} = 50 \text{ kJ}/\text{mol}$ according to Eq. 11.

$$650 \quad D_b(T) = D_b(298 \text{ K}) \cdot \exp \frac{-\Delta H_{\text{dif}}}{R \left(\frac{1}{T} - \frac{1}{298} \right)} \quad (11)$$

Fig. 6 shows that a reduced bulk diffusivity leads to a reduction in peak SOA mass and a shallower evaporation profile. The reduction in SOA yield is caused by a reduction in particle-phase oligomerization: monomer building blocks cannot freely diffuse into the particle, but rather partition to the near-surface layers predominantly. This effectively lowers their uptake coefficient which stands in competition to uptake by the chamber walls. Despite the lower oligomer fraction in these calculations,
 655 evaporation is significantly slowed down compared to the well-mixed case. This model result insinuates that the co-presence of limonene SOA and α -pinene SOA might strongly reduce the mobility of α -pinene oxidation products so that the fast evaporation of α -pinene oxidation products observed in the pure α -pinene oxidation experiment does not take place.

The outcome of this 1-D sensitivity study has to be treated with caution since introducing slow diffusion of oxidation products also causes a shift in all other optimization parameters. For example, with the default parameter set, the slow evaporation
 660 of limonene SOA in the model is purely attributed to oligomer formation. The slow-down in evaporation in this sensitivity study hence suggests that the high oligomerization degree suggested by the model for limonene SOA in the previous best fit solutions might have been overestimated. In fact, a particularly high oligomer content was not observed for limonene SOA from oxidation with NO₃ in measurements using FIGAERO-CIMS (Faxon et al., 2018). Distinction of these two effects (oligomer-

ization vs. mass transfer limitation of slow evaporation) could be possible with the model and the MCGA, but is not attempted
665 in this study due to the prohibitive computational cost of model calculations at low diffusivities and will be subject of future
studies. Furthermore, the slow growth of particles in the pure limonene oxidation experiment is attributed in the well-mixed
model (Sect. 3.1.2) to dissolution and subsequent oligomerization of high volatility compounds in the 4th to 6th volatility bins.
In a viscous particle model, the volatility of these bins might shift down, while maintaining the same particle growth velocity.

We have seen in Sects. 3.2.2 and 3.4, that experimental α -pinene SOA mass can only be matched with a model run that
670 ascribes a high oligomer content to α -pinene SOA (fit 2), which is typically not reported in the literature (Romonosky et al.,
2017). In return, a high oligomer content cannot describe the time evolution of α -pinene pON/OA properly. Hence if, hypothet-
ically, a semi-solid phase state of α -pinene SOA were to slow down evaporation so that SOA evaporation is reconciled between
model and experiment with a particle phase mostly comprised of oligomers, the distinct temporal evolution of pON/OA could
still be matched.

675 Taken together, it is possible that increased mass transfer limitation led to the observed reduced evaporation rates of the
SOA mixtures as postulated in Boyd et al. (2017). However, there are still large uncertainties and a high computational expense
associated with a model treatment of highly viscous SOA systems. While frameworks for the determination of viscosity of
mixtures have recently been developed (Gervasi et al., 2019), these rely on structural information about individual compounds.
Furthermore, while the Stokes-Einstein relation seems to hold for similar systems at viscosities of up to 10^4 Pas (Ullmann
680 et al., 2019), it is not clear whether it also holds for viscosities of 10^7 Pas derived in this study (Evoy et al., 2019).

Additionally, treatment of slow particle-phase diffusion requires many model layers to describe the steep concentrations
gradients arising at the particle surface upon evaporation. In combination with the multitude of tracked species in the particle
phase, computational costs quickly reach unfeasible ranges. Ideally, the spatial resolution model layers would have to be
generated upon model runtime by an algorithm that detects steep concentration gradients. This detailed description will be
685 presented in a forthcoming publication.

4 Conclusions and Outlook

In this study, an inverse modelling approach is utilized alongside laboratory chamber experiments to gain insights into the
molecular-level processes which occur during the formation and evaporation of SOA from the oxidation of α -pinene, limonene,
and mixtures of both precursors with NO_3 . We find α -pinene SOA to form and evaporate rather quickly and limonene SOA
690 to form and evaporate more slowly. Both SOA types, however, show retardation in evaporation compared to instantaneous
equilibration of a specified volatility basis set, which can in part be explained by the presence of particle-phase oligomers.
A mixed and a sequential oxidation of both precursors shows the expected linear additivity of SOA yields, but a non-linear
reduction in evaporation behavior, which could not be fully explained without including diffusion limitations in the particle
phase into the model calculations. Since it is computationally difficult to treat the effects of slow mass transport fully in these
695 models, this paper focuses first on oligomerization and tries to make cases for and against oligomerization as the sole cause for
our observations.

The oxidation products of both SOA types are found to be heavily nitrated. The results highlight the significance of NO₃ as oxidant in SOA formation and the importance of ON as products of monoterpene oxidation. The study finds evidence for non-equilibrium partitioning caused by slow particle-phase chemistry and slow diffusion, which is currently not considered in global models and may lead to underestimation of SOA persistence and hence underestimated global SOA burdens.

The modelling approach applied in this study comprises a combination of the kinetic model based on KM-GAP (Shiraiwa et al., 2012) with the automated global optimization suite MCGA (Berkemeier et al., 2017) and details the full chemistry and physics of SOA particle growth and shrinkage. The underlying SOA formation and evaporation mechanism uses a simplified and lumped version of the Master Chemical Mechanism (MCM; Jenkin et al., 2003; Saunders et al., 2003; Berkemeier et al., 2016), extends it with a reversible particle-phase oligomerization and gas-phase dimerization scheme, and treats gas-particle partitioning with a volatility basis set approach (Donahue et al., 2006, 2011) for each product bin. The study focuses on NO₃ oxidation of monoterpenes and their mixtures, but the model framework can be ported to other chemical systems. The depth resolution capabilities of the model allow for a sensitivity study of the influence of particle phase state on the evaporation of these particles. A full treatment of composition-dependent, depth-resolved viscosity as global optimization parameter is ultimately needed to disentangle the interactions of particle-phase diffusion and particle-phase chemistry. Due to the computational expense of finely-resolved computational layers and the general uncertainty in the physical and chemical parameters, this will be subject of follow-up studies. In such studies, offline analysis of the oligomerization degree of SOA material can help to constrain oligomerization and oligomer decomposition rates and thermodynamic models can be used to provide estimates for composition-dependence of viscosities and diffusivities (DeRieux et al., 2018; Gervasi et al., 2019).

While there is significance to the general conclusions drawn from the model analysis, the individual model parameters that are returned by the inverse modelling approach must be treated with caution and evaluated in the context of the model and experimental data that are employed. Given the large number of fitting parameters and the limited number of experimental data sets, it cannot be insured that a true and correct global minimum is obtained in this isolated case study. With a simplified multi-parameter model and experimental data sets that are aggregate observables and subject to uncertainty, the concept of a single global minimum and multiple local minima on the optimization hypersurface becomes blurred and several extended areas on the optimization hypersurface can exhibit a minimal function value. For example, Fig. S4 shows an estimate of the uncertainty in the volatility distributions obtained in this study. The error bars in Fig. S4 are standard deviations of individual re-fits of volatility distributions that all lead to a similar calculation outcome and hence quantify their uniqueness (or lack thereof). Figs. S1, S8, S9, and S10 show sensitivity case studies of very influential model parameters and Table 1 shows a local sensitivity analysis of the remaining input parameters, which gives an impression of their range within a single model fit. However, the true parameter ranges can be much larger than apparent from these local sensitivity analyses. For example, changes in branching ratios in the gas phase chemical mechanism can in principle be offset with changes in the oxidation products' volatility distributions, thus forming a co-dependent parameter subset. The uniqueness of the obtained parameter set can be enhanced by inclusion of more experimental data at different conditions or by *a priori* determination of model parameters such as measurements of volatility distributions, oligomerization degrees or particle viscosities, which will be an imperative task in follow-up studies.

However, despite the remaining uncertainties in derived model parameters, the modelling suite presented here constitutes a step forward in the computational, data-driven evaluation of SOA formation with kinetic models. In this work, only a small set of laboratory chamber data is utilized for optimization as proof of concept. We postulate that, by reconciling and cross-
735 comparing large sets of experimental data we will be able to significantly enhance our understanding of SOA and close the gap between our expanding theoretical knowledge about the detailed gas-phase chemistry, gas-particle partitioning, particle phase state of SOA, and the application of this knowledge in chemical transport models.

Author contributions. TB and NN designed research. TB, MT, and GE conducted experiments. TB developed the model code and performed simulations. TB, MT, and NN analyzed data. TB prepared the manuscript with contributions from all co-authors.

740 *Competing interests.* The authors declare no conflict of interest.

Acknowledgements. This work was supported by NSF CAREER AGS-1555034. T. Berkemeier acknowledged support by the Eckert Post-doctoral Fellowship from the School of Chemical and Biomolecular Engineering at Georgia Institute of Technology.

References

- Abramson, E., Imre, D., Beranek, J., Wilson, J. M., and Zelenyuk, A.: Experimental determination of chemical diffusion within secondary organic aerosol particles, *Phys. Chem. Chem. Phys.*, 15, 2983–2991, <https://doi.org/10.1039/c2cp44013j>, 2013.
- 745 Atkinson, R. and Arey, J.: Atmospheric Degradation of Volatile Organic Compounds, *Chem. Rev.*, 103, 4605–4638, <https://doi.org/10.1021/cr0206420>, 2003.
- Baltensperger, U., Kalberer, M., Dommen, J., Paulsen, D., Alfarra, M. R., Coe, H., Fisseha, R., Gascho, A., Gysel, M., Nyeki, S., Sax, M., Steinbacher, M., Prevot, A. S. H., Sjögren, S., Weingartner, E., and Zenobi, R.: Secondary organic aerosols from anthropogenic and biogenic precursors, *Faraday Discuss.*, 130, 265–278, <https://doi.org/10.1039/B417367H>, 2005.
- 750 Barsanti, K. C., Kroll, J. H., and Thornton, J. A.: Formation of Low-Volatility Organic Compounds in the Atmosphere: Recent Advancements and Insights, *J. Phys. Chem. Lett.*, 8, 1503–1511, <https://doi.org/10.1021/acs.jpcclett.6b02969>, 2017.
- Berkemeier, T., Huisman, A. J., Ammann, M., Shiraiwa, M., Koop, T., and Pöschl, U.: Kinetic regimes and limiting cases of gas uptake and heterogeneous reactions in atmospheric aerosols and clouds: a general classification scheme, *Atmos. Chem. Phys.*, 13, 6663–6686, <https://doi.org/10.5194/acp-13-6663-2013>, 2013.
- 755 Berkemeier, T., Ammann, M., Mentel, T. F., Pöschl, U., and Shiraiwa, M.: Organic Nitrate Contribution to New Particle Formation and Growth in Secondary Organic Aerosols from α -Pinene Ozonolysis, *Environ. Sci. Technol.*, 50, 6334–6342, <https://doi.org/10.1021/acs.est.6b00961>, 2016.
- Berkemeier, T., Ammann, M., Krieger, U. K., Peter, T., Spichtinger, P., Pöschl, U., Shiraiwa, M., and Huisman, A. J.: Technical note: Monte Carlo genetic algorithm (MCGA) for model analysis of multiphase chemical kinetics to determine transport and reaction rate coefficients using multiple experimental data sets, *Atmos. Chem. Phys.*, 17, 8021–8029, <https://doi.org/10.5194/acp-17-8021-2017>, 2017.
- 760 Berndt, T., Mentler, B., Scholz, W., Fischer, L., Herrmann, H., Kulmala, M., and Hansel, A.: Accretion Product Formation from Ozonolysis and OH Radical Reaction of α -Pinene: Mechanistic Insight and the Influence of Isoprene and Ethylene, *Environ. Sci. Technol.*, 52, 11 069–11 077, <https://doi.org/10.1021/acs.est.8b02210>, 2018.
- 765 Boyd, C. M., Sanchez, J., Xu, L., Eugene, A. J., Nah, T., Tuet, W. Y., Guzman, M. I., and Ng, N. L.: Secondary organic aerosol formation from the beta-pinene+NO₃ system: effect of humidity and peroxy radical fate, *Atmos. Chem. Phys.*, 15, 7497–7522, <https://doi.org/10.5194/acp-15-7497-2015>, 2015.
- Boyd, C. M., Nah, T., Xu, L., Berkemeier, T., and Ng, N. L.: Secondary Organic Aerosol (SOA) from Nitrate Radical Oxidation of Monoterpenes: Effects of Temperature, Dilution, and Humidity on Aerosol Formation, Mixing, and Evaporation, *Environ. Sci. Technol.*, 51, 7831–7841, <https://doi.org/10.1021/acs.est.7b01460>, 2017.
- 770 Canagaratna, M., Jayne, J., Jimenez, J., Allan, J., Alfarra, M., Zhang, Q., Onasch, T., Drewnick, F., Coe, H., Middlebrook, A., Delia, A., Williams, L., Trimborn, A., Northway, M., DeCarlo, P., Kolb, C., Davidovits, P., and Worsnop, D.: Chemical and microphysical characterization of ambient aerosols with the aerodyne aerosol mass spectrometer, *Mass Spectrom. Rev.*, 26, 185–222, <https://doi.org/10.1002/mas.20115>, 2007.
- Cappa, C. D. and Wilson, K. R.: Evolution of organic aerosol mass spectra upon heating: implications for OA phase and partitioning behavior, *Atmos. Chem. Phys.*, 11, 1895–1911, <https://doi.org/10.5194/acp-11-1895-2011>, 2011.
- Chung, S. H. and Seinfeld, J. H.: Global distribution and climate forcing of carbonaceous aerosols, *J. Geophys. Res. Atmospheres*, 107, <https://doi.org/10.1029/2001jd001397>, 2002.

- 780 Clafin, M. S. and Ziemann, P. J.: Identification and Quantitation of Aerosol Products of the Reaction of β -Pinene with NO₃ Radicals and Implications for Gas- and Particle-Phase Reaction Mechanisms, *J. Phys. Chem. A*, 122, 3640–3652, <https://doi.org/10.1021/acs.jpca.8b00692>, 2018.
- DeCarlo, P. F., Kimmel, J. R., Trimborn, A., Northway, M. J., Jayne, J. T., Aiken, A. C., Gonin, M., Fuhrer, K., Horvath, T., Docherty, K. S., Worsnop, D. R., and Jimenez, J. L.: Field-Deployable, High-Resolution, Time-of-Flight Aerosol Mass Spectrometer, *Anal. Chem.*, 78, 8281–8289, <https://doi.org/10.1021/ac061249n>, 2006.
- 785 DePalma, J. W., Horan, A. J., Hall IV, W. A., and Johnston, M. V.: Thermodynamics of oligomer formation: implications for secondary organic aerosol formation and reactivity, *Phys. Chem. Chem. Phys.*, 15, 6935–6944, <https://doi.org/10.1039/C3CP44586K>, 2013.
- DeRieux, W. S. W., Li, Y., Lin, P., Laskin, J., Laskin, A., Bertram, A. K., Nizkorodov, S. A., and Shiraiwa, M.: Predicting the glass transition temperature and viscosity of secondary organic material using molecular composition, *Atmos. Chem. Phys.*, 18, 6331–6351, <https://doi.org/10.5194/acp-18-6331-2018>, 2018.
- 790 Donahue, N. M., Robinson, A. L., Stanier, C. O., and Pandis, S. N.: Coupled partitioning, dilution, and chemical aging of semivolatile organics, *Environ. Sci. Technol.*, 40, 2635–2643, <https://doi.org/10.1021/es052297c>, 2006.
- Donahue, N. M., Epstein, S. A., Pandis, S. N., and Robinson, A. L.: A two-dimensional volatility basis set: 1. organic-aerosol mixing thermodynamics, *Atmos. Chem. Phys.*, 11, 3303–3318, <https://doi.org/10.5194/acp-11-3303-2011>, 2011.
- Draper, D. C., Myllys, N., Hyttinen, N., Møller, K. H., Kjaergaard, H. G., Fry, J. L., Smith, J. N., and Kurtén, T.: Formation of Highly Oxidized Molecules from NO₃ Radical Initiated Oxidation of Δ -3-Carene: A Mechanistic Study, *ACS Earth Space Chem.*, 3, 1460–1470, <https://doi.org/10.1021/acsearthspacechem.9b00143>, 2019.
- 795 D'Ambro, E. L., Schobesberger, S., Zaveri, R. A., Shilling, J. E., Lee, B. H., Lopez-Hilfiker, F. D., Mohr, C., and Thornton, J. A.: Isothermal Evaporation of α -Pinene Ozonolysis SOA: Volatility, Phase State, and Oligomeric Composition, *ACS Earth Space Chem.*, 2, 1058–1067, <https://doi.org/10.1021/acsearthspacechem.8b00084>, 2018.
- 800 Einstein, A.: Über die von der molekularkinetischen Theorie der Wärme geforderte Bewegung von in ruhenden Flüssigkeiten suspendierten Teilchen, *Ann. Phys.*, 322, 549–560, <https://doi.org/10.1002/andp.19053220806>, 1905.
- Evoy, E., Maclean, A. M., Rovelli, G., Li, Y., Tsimpidi, A. P., Karydis, V. A., Kamal, S., Lelieveld, J., Shiraiwa, M., Reid, J. P., and Bertram, A. K.: Predictions of diffusion rates of large organic molecules in secondary organic aerosols using the Stokes–Einstein and fractional Stokes–Einstein relations, *Atmos. Chem. Phys.*, 19, 10 073–10 085, <https://doi.org/10.5194/acp-19-10073-2019>, 2019.
- 805 Faxon, C., Hammes, J., Le Breton, M., Pathak, R. K., and Hallquist, M.: Characterization of organic nitrate constituents of secondary organic aerosol (SOA) from nitrate-radical-initiated oxidation of limonene using high-resolution chemical ionization mass spectrometry, *Atmos. Chem. Phys.*, 18, 5467–5481, <https://doi.org/10.5194/acp-18-5467-2018>, 2018.
- Fry, J. L., Kiendler-Scharr, A., Rollins, A. W., Wooldridge, P. J., Brown, S. S., Fuchs, H., Dubé, W., Mensah, A., dal Maso, M., Tillmann, R., Dorn, H. P., Brauers, T., and Cohen, R. C.: Organic nitrate and secondary organic aerosol yield from NO₃ oxidation of β -pinene evaluated using a gas-phase kinetics/aerosol partitioning model, *Atmos. Chem. Phys.*, 9, 1431–1449, <https://doi.org/10.5194/acp-9-1431-2009>, 2009.
- 810 Fry, J. L., Kiendler-Scharr, A., Rollins, A. W., Brauers, T., Brown, S. S., Dorn, H. P., Dubé, W. P., Fuchs, H., Mensah, A., Rohrer, F., Tillmann, R., Wahner, A., Wooldridge, P. J., and Cohen, R. C.: SOA from limonene: role of NO₃ in its generation and degradation, *Atmos. Chem. Phys.*, 11, 3879–3894, <https://doi.org/10.5194/acp-11-3879-2011>, 2011.

- 815 Fry, J. L., Draper, D. C., Barsanti, K. C., Smith, J. N., Ortega, J., Winkler, P. M., Lawler, M. J., Brown, S. S., Edwards, P. M., Cohen, R. C., and Lee, L.: Secondary Organic Aerosol Formation and Organic Nitrate Yield from NO₃ Oxidation of Biogenic Hydrocarbons, *Environ. Sci. Technol.*, 48, 11 944–11 953, <https://doi.org/10.1021/es502204x>, 2014.
- Fuzzi, S., Andreae, M. O., Huebert, B. J., Kulmala, M., Bond, T. C., Boy, M., Doherty, S. J., Guenther, A., Kanakidou, M., Kawamura, K., Kerminen, V. M., Lohmann, U., Russell, L. M., and Pöschl, U.: Critical assessment of the current state of scientific knowledge, terminology, and research needs concerning the role of organic aerosols in the atmosphere, climate, and global change, *Atmos. Chem. Phys.*, 6, 2017–2038, <https://doi.org/10.5194/acp-6-2017-2006>, 2006.
- 820 Gao, Y., Hall, W. A., and Johnston, M. V.: Molecular Composition of Monoterpene Secondary Organic Aerosol at Low Mass Loading, *Environ. Sci. Technol.*, 44, 7897–7902, <https://doi.org/10.1021/es101861k>, 2010.
- Gatzsche, K., Iinuma, Y., Tilgner, A., Mutzel, A., Berndt, T., and Wolke, R.: Kinetic modeling studies of SOA formation from α -pinene ozonolysis, *Atmos. Chem. Phys.*, 17, 13 187–13 211, <https://doi.org/10.5194/acp-17-13187-2017>, 2017.
- 825 Gervasi, N. R., Topping, D. O., and Zuend, A.: A predictive group-contribution model for the viscosity of aqueous organic aerosol, *Atmos. Chem. Phys. Discuss.*, 2019, 1–32, <https://doi.org/10.5194/acp-2019-699>, 2019.
- Grayson, J. W., Zhang, Y., Mutzel, A., Renbaum-Wolff, L., Böge, O., Kamal, S., Herrmann, H., Martin, S. T., and Bertram, A. K.: Effect of varying experimental conditions on the viscosity of α -pinene derived secondary organic material, *Atmos. Chem. Phys.*, 16, 6027–6040, <https://doi.org/10.5194/acp-16-6027-2016>, 2016.
- 830 Hallquist, M., Wängberg, I., Ljungström, E., Barnes, I., and Becker, K.-H.: Aerosol and Product Yields from NO₃ Radical-Initiated Oxidation of Selected Monoterpenes, *Environ. Sci. Technol.*, 33, 553–559, <https://doi.org/10.1021/es980292s>, 1999.
- Hallquist, M., Wenger, J. C., Baltensperger, U., Rudich, Y., Simpson, D., Claeys, M., Dommen, J., Donahue, N. M., George, C., Goldstein, A. H., Hamilton, J. F., Herrmann, H., Hoffmann, T., Iinuma, Y., Jang, M., Jenkin, M. E., Jimenez, J. L., Kiendler-Scharr, A., Maenhaut, W., McFiggans, G., Mentel, T. F., Monod, A., Prevot, A. S. H., Seinfeld, J. H., Surratt, J. D., Szmigielski, R., and Wildt, J.: The formation, properties and impact of secondary organic aerosol: current and emerging issues, *Atmos. Chem. Phys.*, 9, 5155–5235, <https://doi.org/10.5194/acp-9-5155-2009>, 2009.
- 835 Huang, Y., Zhao, R., Charan, S. M., Kenseth, C. M., Zhang, X., and Seinfeld, J. H.: Unified Theory of Vapor–Wall Mass Transport in Teflon-Walled Environmental Chambers, *Environ. Sci. Technol.*, 52, 2134–2142, <https://doi.org/10.1021/acs.est.7b05575>, 2018.
- 840 Jenkin, M. E., Saunders, S. M., Wagner, V., and Pilling, M. J.: Protocol for the development of the Master Chemical Mechanism, MCM v3 (Part B): tropospheric degradation of aromatic volatile organic compounds, *Atmos. Chem. Phys.*, 3, 181–193, <https://doi.org/10.5194/acp-3-181-2003>, 2003.
- Julin, J., Shiraiwa, M., Miles, R. E. H., Reid, J. P., Pöschl, U., and Riipinen, I.: Mass Accommodation of Water: Bridging the Gap Between Molecular Dynamics Simulations and Kinetic Condensation Models, *J. Phys. Chem. A*, 117, 410–420, <https://doi.org/10.1021/jp310594e>, 2013.
- 845 Kalberer, M., Paulsen, D., Sax, M., Steinbacher, M., Dommen, J., Prevot, A. S. H., Fisseha, R., Weingartner, E., Frankevich, V., Zenobi, R., and Baltensperger, U.: Identification of polymers as major components of atmospheric organic aerosols, *Science*, 303, 1659–1662, <https://doi.org/10.1126/science.1092185>, 2004.
- Kanakidou, M., Seinfeld, J. H., Pandis, S. N., Barnes, I., Dentener, F. J., Facchini, M. C., Van Dingenen, R., Ervens, B., Nenes, A., Nielsen, C. J., Swietlicki, E., Putaud, J. P., Balkanski, Y., Fuzzi, S., Horth, J., Moortgat, G. K., Winterhalter, R., Myhre, C. E. L., Tsigaridis, K., Vignati, E., Stephanou, E. G., and Wilson, J.: Organic aerosol and global climate modelling: a review, *Atmos. Chem. Phys.*, 5, 1053–1123, <https://doi.org/10.5194/acp-5-1053-2005>, 2005.

- Keyword, M. D., Varutbangkul, V., Bahreini, R., Flagan, R. C., and Seinfeld, J. H.: Secondary organic aerosol formation from the ozonolysis of cycloalkenes and related compounds, *Environ. Sci. Technol.*, 38, 4157–4164, <https://doi.org/10.1021/es.035363o>, 2004.
- 855 Koop, T., Bookhold, J., Shiraiwa, M., and Pöschl, U.: Glass transition and phase state of organic compounds: dependency on molecular properties and implications for secondary organic aerosols in the atmosphere, *Phys. Chem. Chem. Phys.*, 13, 19238–19255, <https://doi.org/10.1039/C1CP22617G>, 2011.
- Kurtén, T., Møller, K. H., Nguyen, T. B., Schwantes, R. H., Misztal, P. K., Su, L., Wennberg, P. O., Fry, J. L., and Kjaergaard, H. G.: Alkoxy Radical Bond Scissions Explain the Anomalously Low Secondary Organic Aerosol and Organonitrate Yields From α -Pinene + NO₃, *J. Phys. Chem. Lett.*, 8, 2826–2834, <https://doi.org/10.1021/acs.jpcclett.7b01038>, 2017.
- 860 Liebmann, J., Sobanski, N., Schuladen, J., Karu, E., Hellén, H., Hakola, H., Zha, Q., Ehn, M., Riva, M., Heikkinen, L., Williams, J., Fischer, H., Lelieveld, J., and Crowley, J. N.: Alkyl nitrates in the boreal forest: formation via the NO₃-, OH- and O₃-induced oxidation of biogenic volatile organic compounds and ambient lifetimes, *Atmos. Chem. Phys.*, 19, 10391–10403, <https://doi.org/10.5194/acp-19-10391-2019>, 2019.
- 865 Lopez-Hilfiker, F. D., Mohr, C., Ehn, M., Rubach, F., Kleist, E., Wildt, J., Mentel, T. F., Lutz, A., Hallquist, M., Worsnop, D., and Thornton, J. A.: A novel method for online analysis of gas and particle composition: description and evaluation of a Filter Inlet for Gases and AEROSols (FIGAERO), *Atmos. Meas. Tech.*, 7, 983–1001, <https://doi.org/10.5194/amt-7-983-2014>, 2014.
- Marshall, F. H., Berkemeier, T., Shiraiwa, M., Nandy, L., Ohm, P. B., Dutcher, C. S., and Reid, J. P.: Influence of particle viscosity on mass transfer and heterogeneous ozonolysis kinetics in aqueous–sucrose–maleic acid aerosol, *Phys. Chem. Chem. Phys.*, 20, 15560–15573, <https://doi.org/10.1039/C8CP01666F>, 2018.
- 870 Müller, J. F., Peeters, J., and Stavrou, T.: Fast photolysis of carbonyl nitrates from isoprene, *Atmos. Chem. Phys.*, 14, 2497–2508, <https://doi.org/10.5194/acp-14-2497-2014>, 2014.
- Nah, T., McVay, R. C., Zhang, X., Boyd, C. M., Seinfeld, J. H., and Ng, N. L.: Influence of seed aerosol surface area and oxidation rate on vapor wall deposition and SOA mass yields: a case study with α -pinene ozonolysis, *Atmos. Chem. Phys.*, 16, 9361–9379, <https://doi.org/10.5194/acp-16-9361-2016>, 2016a.
- 875 Nah, T., Sanchez, J., Boyd, C. M., and Ng, N. L.: Photochemical Aging of α -pinene and β -pinene Secondary Organic Aerosol formed from Nitrate Radical Oxidation, *Environ. Sci. Technol.*, 50, 222–231, <https://doi.org/10.1021/acs.est.5b04594>, 2016b.
- Nah, T., McVay, R. C., Pierce, J. R., Seinfeld, J. H., and Ng, N. L.: Constraining uncertainties in particle-wall deposition correction during SOA formation in chamber experiments, *Atmos. Chem. Phys.*, 17, 2297–2310, <https://doi.org/10.5194/acp-17-2297-2017>, 2017.
- 880 Ng, N. L., Brown, S. S., Archibald, A. T., Atlas, E., Cohen, R. C., Crowley, J. N., Day, D. A., Donahue, N. M., Fry, J. L., Fuchs, H., Griffin, R. J., Guzman, M. I., Herrmann, H., Hodzic, A., Iinuma, Y., Jimenez, J. L., Kiendler-Scharr, A., Lee, B. H., Luecken, D. J., Mao, J., McLaren, R., Mutzel, A., Osthoff, H. D., Ouyang, B., Picquet-Varrault, B., Platt, U., Pye, H. O. T., Rudich, Y., Schwantes, R. H., Shiraiwa, M., Stutz, J., Thornton, J. A., Tilgner, A., Williams, B. J., and Zaveri, R. A.: Nitrate radicals and biogenic volatile organic compounds: oxidation, mechanisms, and organic aerosol, *Atmos. Chem. Phys.*, 17, 2103–2162, <https://doi.org/10.5194/acp-17-2103-2017>, 2017.
- 885 Nguyen, T. B., Crounse, J. D., Teng, A. P., St. Clair, J. M., Paulot, F., Wolfe, G. M., and Wennberg, P. O.: Rapid deposition of oxidized biogenic compounds to a temperate forest, *Proc. Natl. Acad. Sci. USA*, 112, E392, <https://doi.org/10.1073/pnas.1418702112>, 2015.
- Pankow, J. F.: An absorption model of gas-particle partitioning of organic-compounds in the atmosphere, *Atmos. Env.*, 28, 185–188, 1994.
- Perring, A. E., Pusede, S. E., and Cohen, R. C.: An Observational Perspective on the Atmospheric Impacts of Alkyl and Multifunctional Nitrates on Ozone and Secondary Organic Aerosol, *Chem. Rev.*, 113, 5848–5870, <https://doi.org/10.1021/cr300520x>, 2013.

- 890 Pöschl, U.: Atmospheric aerosols: Composition, transformation, climate and health effects, *Angew. Chem. Int. Ed.*, 44, 7520–7540, <https://doi.org/10.1002/anie.200501122>, 2005.
- Press, W. H., Teukolsky, S. A., Vetterling, W. T., and Flannery, B. P.: *Numerical Recipes 3rd Edition: The Art of Scientific Computing*, Cambridge University Press, 2007.
- Reid, J. P., Bertram, A. K., Topping, D. O., Laskin, A., Martin, S. T., Petters, M. D., Pope, F. D., and Rovelli, G.: The viscosity of atmospher-
895 ically relevant organic particles, *Nature Comm.*, 9, 956, <https://doi.org/10.1038/s41467-018-03027-z>, 2018.
- Roldin, P., Eriksson, A. C., Nordin, E. Z., Hermansson, E., Mogensen, D., Rusanen, A., Boy, M., Swietlicki, E., Svenningsson, B., Zelenyuk, A., and Pagels, J.: Modelling non-equilibrium secondary organic aerosol formation and evaporation with the aerosol dynamics, gas- and particle-phase chemistry kinetic multilayer model ADCHAM, *Atmos. Chem. and Phys.*, 14, 7953–7993, <https://doi.org/10.5194/acp-14-7953-2014>, 2014.
- 900 Romonosky, D. E., Li, Y., Shiraiwa, M., Laskin, A., Laskin, J., and Nizkorodov, S. A.: Aqueous Photochemistry of Secondary Organic Aerosol of α -Pinene and α -Humulene Oxidized with Ozone, Hydroxyl Radical, and Nitrate Radical, *J. Phys. Chem. A*, 121, 1298–1309, <https://doi.org/10.1021/acs.jpca.6b10900>, 2017.
- Saathoff, H., Naumann, K. H., Möhler, O., Jonsson, A. M., Hallquist, M., Kiendler-Scharr, A., Mentel, T. F., Tillmann, R., and Schurath, U.: Temperature dependence of yields of secondary organic aerosols from the ozonolysis of α -pinene and limonene, *Atmos. Chem. Phys.*, 9,
905 1551–1577, <https://doi.org/10.5194/acp-9-1551-2009>, 2009.
- Saunders, S. M., Jenkin, M. E., Derwent, R. G., and Pilling, M. J.: Protocol for the development of the Master Chemical Mechanism, MCM v3 (Part A): tropospheric degradation of non-aromatic volatile organic compounds, *Atmos. Chem. Phys.*, 3, 161–180, <https://doi.org/10.5194/acp-3-161-2003>, 2003.
- Seinfeld, J. H. and Pandis, S. N.: *Atmos. Chem. Phys.: From Air Pollution to Climate Change*, John Wiley & Sons, Inc., New York, 2016.
- 910 Shiraiwa, M., Pfrang, C., and Pöschl, U.: Kinetic multi-layer model of aerosol surface and bulk chemistry (KM-SUB): the influence of interfacial transport and bulk diffusion on the oxidation of oleic acid by ozone, *Atmos. Chem. Phys.*, 10, 3673–3691, <https://doi.org/10.5194/acp-10-3673-2010>, 2010.
- Shiraiwa, M., Ammann, M., Koop, T., and Pöschl, U.: Gas uptake and chemical aging of semisolid organic aerosol particles, *Proc. Natl. Acad. Sci. USA*, 108, 11 003–11 008, <https://doi.org/10.1073/pnas.1103045108>, 2011.
- 915 Shiraiwa, M., Pfrang, C., Koop, T., and Pöschl, U.: Kinetic multi-layer model of gas-particle interactions in aerosols and clouds (KM-GAP): linking condensation, evaporation and chemical reactions of organics, oxidants and water, *Atmos. Chem. Phys.*, 12, 2777–2794, <https://doi.org/10.5194/acp-12-2777-2012>, 2012.
- Shiraiwa, M., Yee, L. D., Schilling, K. A., Loza, C. L., Craven, J. S., Zuend, A., Ziemann, P. J., and Seinfeld, J. H.: Size distribution dynamics reveal particle-phase chemistry in organic aerosol formation, *Proc. Natl. Acad. Sci. USA*, 110, 11 746–11 750,
920 <https://doi.org/10.1073/pnas.1307501110>, 2013.
- Takeuchi, M. and Ng, N. L.: Chemical composition and hydrolysis of organic nitrate aerosol formed from hydroxyl and nitrate radical oxidation of α -pinene and β -pinene, *Atmos. Chem. Phys.*, 19, 12 749–12 766, <https://doi.org/10.5194/acp-19-12749-2019>, 2019.
- Tikkanen, O. P., Hämäläinen, V., Rovelli, G., Lipponen, A., Shiraiwa, M., Reid, J. P., Lehtinen, K. E. J., and Yli-Juuti, T.: Optimization of process models for determining volatility distribution and viscosity of organic aerosols from isothermal particle evaporation data, *Atmos. Chem. Phys.*, 19, 9333–9350, <https://doi.org/10.5194/acp-19-9333-2019>, 2019.
- 925 Tsigaridis, K., Krol, M., Dentener, F. J., Balkanski, Y., Lathièrre, J., Metzger, S., Hauglustaine, D. A., and Kanakidou, M.: Change in global aerosol composition since preindustrial times, *Atmos. Chem. Phys.*, 6, 5143–5162, <https://doi.org/10.5194/acp-6-5143-2006>, 2006.

- Ullmann, D. A., Hinks, M. L., Maclean, A. M., Butenhoff, C. L., Grayson, J. W., Barsanti, K., Jimenez, J. L., Nizkorodov, S. A., Kamal, S., and Bertram, A. K.: Viscosities, diffusion coefficients, and mixing times of intrinsic fluorescent organic molecules in brown limonene secondary organic aerosol and tests of the Stokes–Einstein equation, *Atmos. Chem. Phys.*, 19, 1491–1503, <https://doi.org/10.5194/acp-19-1491-2019>, 2019.
- 930 Vaden, T. D., Imre, D., Beranek, J., Shrivastava, M., and Zelenyuk, A.: Evaporation kinetics and phase of laboratory and ambient secondary organic aerosol, *Proc. Natl. Sci. Acad. USA*, 108, 2190–2195, <https://doi.org/10.1073/pnas.1013391108>, 2011.
- Vereecken, L., Müller, J.-F., and Peeters, J.: Low-volatility poly-oxygenates in the OH-initiated atmospheric oxidation of α -pinene: impact of non-traditional peroxy radical chemistry, *Phys. Chem. Chem. Phys.*, 9, 5241–5248, <https://doi.org/10.1039/B708023A>, 2007.
- 935 Virtanen, A., Joutsensaari, J., Koop, T., Kannosto, J., YliPirilä, P., Leskinen, J., Mäkelä, J. M., Holopainen, J. K., Pöschl, U., Kulmala, M., Worsnop, D. R., and Laaksonen, A.: An amorphous solid state of biogenic secondary organic aerosol particles, *Nature*, 467, 824–827, <https://doi.org/doi:10.1038/nature09455>, 2010.
- von Domaros, M., Lakey, P. S. J., Shiraiwa, M., and Tobias, D. J.: Multiscale Modeling of Human Skin Oil-Induced Indoor Air Chemistry: Combining Kinetic Models and Molecular Dynamics, *J. Phys. Chem. B.*, 124, 3836–3843, <https://doi.org/10.1021/acs.jpcc.0c02818>, 2020.
- 940 Yli-Juuti, T., Pajunoja, A., Tikkanen, O.-P., Buchholz, A., Faiola, C., Väisänen, O., Hao, L., Kari, E., Peräkylä, O., Garmash, O., Shiraiwa, M., Ehn, M., Lehtinen, K., and Virtanen, A.: Factors controlling the evaporation of secondary organic aerosol from α -pinene ozonolysis, *Geophys. Res. Lett.*, 44, 2562–2570, <https://doi.org/10.1002/2016GL072364>, 2017.
- Zaveri, R. A., Easter, R. C., Fast, J. D., and Peters, L. K.: Model for Simulating Aerosol Interactions and Chemistry (MOSAIC), *J. Geophys. Res. Atmospheres*, 113, <https://doi.org/10.1029/2007jd008782>, 2008.
- 945 Zaveri, R. A., Easter, R. C., Shilling, J. E., and Seinfeld, J. H.: Modeling kinetic partitioning of secondary organic aerosol and size distribution dynamics: representing effects of volatility, phase state, and particle-phase reaction, *Atmos. Chem. Phys.*, 14, 5153–5181, <https://doi.org/10.5194/acp-14-5153-2014>, 2014.
- Zaveri, R. A., Shilling, J. E., Zelenyuk, A., Liu, J., Bell, D. M., D’Ambro, E. L., Gaston, C. J., Thornton, J. A., Laskin, A., Lin, P., Wilson, J., Easter, R. C., Wang, J., Bertram, A. K., Martin, S. T., Seinfeld, J. H., and Worsnop, D. R.: Growth Kinetics and Size Distribution Dynamics of Viscous Secondary Organic Aerosol, *Environ. Sci. Technol.*, 52, 1191–1199, <https://doi.org/10.1021/acs.est.7b04623>, 2018.
- 950 Zhang, Y., Sanchez, M. S., Douet, C., Wang, Y., Bateman, A. P., Gong, Z., Kuwata, M., Renbaum-Wolff, L., Sato, B. B., Liu, P. F., Bertram, A. K., Geiger, F. M., and Martin, S. T.: Changing shapes and implied viscosities of suspended submicron particles, *Atmos. Chem. Phys.*, 15, 7819–7829, <https://doi.org/10.5194/acp-15-7819-2015>, 2015.
- 955 Ziemann, P. J. and Atkinson, R.: Kinetics, products, and mechanisms of secondary organic aerosol formation, *Chem. Soc. Rev.*, 41, 6582–6605, <https://doi.org/10.1039/c2cs35122f>, 2012.